



## REVIEW

[View Article Online](#)  
[View Journal](#) | [View Issue](#)Cite this: *Mater. Horiz.*, 2025,  
12, 64

# Graphene-based polymer composites in thermal management: materials, structures and applications

Luqi Liu,<sup>ab</sup> Chenchen Xu,<sup>a</sup> Yuequan Yang,<sup>a</sup> Chao Fu,<sup>a</sup> Fuliang Ma,<sup>a</sup>  
Zhixiang Zeng <sup>\*a</sup> and Gang Wang <sup>\*a</sup>

Graphene, with its high thermal conductivity ( $k$ ), excellent mechanical properties, and thermal stability, is an ideal filler for developing advanced high  $k$  and heat dissipation materials. However, creating graphene-based polymer nanocomposites (GPNs) with high  $k$  remains a significant challenge to meet the demand for efficient heat dissipation. Here, the effects of graphene material and structure on thermal properties are investigated from both microscopic and macroscopic perspectives. Initially, it briefly introduces the influence of graphene structural parameters on its intrinsic  $k$ , along with summarizing methods to adjust these parameters. Various techniques for establishing different thermal conductivity pathways at the macroscopic scale (including filler hybridization, 3D networks, horizontal alignment, and vertical alignment) are reviewed, along with their respective advantages and disadvantages. Furthermore, we discuss the applications of GPNs as thermal interface materials (TIMs), phase change materials (PCMs), and smart responsive thermal management materials in the field of thermal management. Finally, the current challenges and future perspectives of GPN research are discussed. This review offers researchers a comprehensive overview of recent advancements in GPNs for thermal management and guidance for developing the next generation of thermally conductive polymer composites.

Received 30th June 2024,  
Accepted 30th September 2024

DOI: 10.1039/d4mh00846d

[rsc.li/materials-horizons](https://rsc.li/materials-horizons)

## Wider impact

Graphene is considered the ideal thermally conductive filler for addressing heat accumulation in polymeric materials, owing to its high theoretical  $k$ . However, inefficient and low-quality graphene preparation, along with challenges in dispersion, significantly hinder the progress of GPNs in thermal management. Consequently, recent efforts have focused on producing high-quality graphene in various shapes and sizes, as well as creating graphene pathways with different alignments to achieve GPNs with superior  $k$  and mechanical properties. A deep understanding of thermal conductivity mechanisms, preparation techniques, and the design of macroscopic thermally conductive structures is crucial for obtaining optimal graphene and GPNs. This review comprehensively investigates the impact of graphene material and structure on thermal properties from both microscopic and macroscopic viewpoints, comparing the pros and cons of different methods for creating thermally conductive pathways in detail. Furthermore, it highlights cutting-edge applications of GPNs in thermal management, while also addressing current research challenges and opportunities. The insights presented in this review aim to equip researchers with a thorough understanding of recent advancements in GPNs for thermal management and offer insights for the development of the next generation of thermally conductive polymer composites.

## 1. Introduction

The progressively high heat flow density of electronic devices poses a great challenge to current thermal dissipation

technologies.<sup>1–3</sup> The 10 °C rule suggests that a 10 °C increase in the operating temperature of a single electronic device results in a 50% reduction in reliability.<sup>4</sup> Therefore, there is an urgent need for efficient thermal management materials to address these issues. Polymer materials (both thermoset and thermoplastic, such as epoxy (EP), polystyrene, polycarbonate, polyurethane (PU), polyimide (PI), polyethylene, nylon, etc.) are widely used for thermal management because of their flexibility, insulating properties, processability, and light weight.<sup>5</sup> However, their low  $k$  (approximately 0.1–0.5 W m<sup>−1</sup> K<sup>−1</sup>)

<sup>a</sup> Key Laboratory of Advanced Marine Materials, Ningbo Institute of Materials Technology and Engineering, Chinese Academy of Sciences, Ningbo 315201, P. R. China. E-mail: zengzhx@nimte.ac.cn, wanggang@nimte.ac.cn

<sup>b</sup> Center of Materials Science and Optoelectronics Engineering, University of Chinese Academy of Sciences, Beijing 100049, P. R. China

severely limits the rapid development of polymeric materials for thermal management.<sup>6,7</sup>

Graphene is a 2D material with outstanding physical and chemical properties, including high  $k$  ( $\sim 5000 \text{ W m}^{-1} \text{ K}^{-1}$ ), high surface area ( $\sim 2600 \text{ m}^2 \text{ g}^{-1}$ ), excellent mechanical properties (mechanical strength of 130 GPa), and thermal stability.<sup>8–10</sup> It has promising applications in aerospace,<sup>11,12</sup> energy harvesting systems,<sup>13</sup> energy storage devices,<sup>14</sup> and wearable electronics.<sup>15</sup> In the past decade, graphene and its derivatives have been proven to be very effective in enhancing the  $k$  of various polymers by many researchers.<sup>16–18</sup> However, due to its large specific surface area and strong  $\pi$ - $\pi$  interactions, graphene tends to aggregate and stack together in a way that is difficult to disperse effectively, limiting its use in polymeric materials.<sup>19–22</sup> Structural design of graphene is considered a feasible strategy to fully utilize the advantages of graphene and overcome its disadvantage of difficult dispersion.<sup>23,24</sup> In addition, the presence of numerous interfaces in GPNs with nano-scale dimensions results in complex heat transfer phenomena. Consequently, a significant number of studies have focused on elucidating the heat transfer mechanisms of graphene nanofillers in polymers and exploring strategies to enhance the  $k$  of GPNs.<sup>16,25</sup> Meanwhile, increasing  $k$  of GPNs while maintaining other advantageous characteristics is a major challenge at present.<sup>26</sup>

While previous studies have summarized the factors influencing the  $k$  and the thermal conductivity mechanism in GPNs, few articles have analyzed the effect of different states of graphene in the polymer matrix on the thermal properties of the composites from the microscopic to macroscopic viewpoints. The different states of graphene at different scales lead to significant differences in the thermal properties of the materials. This work centers around this graphene-induced variability in material properties. First, the influence of structural parameters of graphene (defects, size, number of layers, *etc.*) on the microscopic intrinsic  $k$  of graphene is analyzed, and the current common methods and strategies to modulate these parameters, such as exfoliation of graphene preparation and defect engineering, are summarized. Different surface modifications of graphene are also proposed to address the issue of high interfacial thermal resistance, which arises from poor dispersion and weak contact between graphene and polymer. Subsequently, the effects of different macroscopic polymers formed by graphene with different pathway structures (mainly including hybridized structures of graphene with other materials, 3D graphene networks, and graphene horizontally aligned and vertically aligned) on the thermal properties of the materials are analyzed. Finally, the value of GPNs as TIM, phase change cooling materials, and smart responsive materials for engineering thermal management applications is emphasized, respectively. It is hoped that this work will help researchers gain a deeper understanding of the heat transfer mechanism of GPNs, the laws affecting the thermal properties, and the cutting-edge applications in thermal management, and provide assistance in the subsequent research on GPNs.

## 2. Peculiarity of graphene material

### 2.1 Heat transfer mechanism of graphene

The main modes of heat transfer in solids include electronic and phonon conduction. The vibration of the lattice structure plays a decisive role in the heat transfer process for electrically insulating solid materials.<sup>27</sup> The process by which an atom undergoes thermal vibrations to transfer energy to neighboring atoms is illustrated in Fig. 1(a). The quantized lattice vibrational energy is called a phonon and can be understood as similar to a photon. The Debye equation shows that the  $k$  of a polymer material is proportional to the volumetric heat capacity of materials, the velocity of the phonon group, and the mean free path of the phonons.<sup>28</sup> To enhance the  $k$  of a material, one can start by enhancing the velocity and the mean free path of the phonon group. Graphene is a 2D material composed of  $\text{sp}^2$  hybridized carbon atoms with extremely high specific surface area and a unique six-membered carbocyclic conjugated large  $\pi$ -bonding structure (Fig. 1(b)).<sup>29</sup> The  $k$  of graphene is mainly contributed by phonons, transferring energy in a ballistic-diffusive manner.<sup>30</sup> The  $k$  of free monolayer graphene has an ultra-high  $k$  of  $5.0 \times 10^3 \text{ W m}^{-1} \text{ K}^{-1}$  at room temperature, which is much higher than that of other common materials (Table 1). The fundamental reason for the extremely high  $k$  of graphene is that it has a 2D honeycomb lattice structure, which facilitates a significant reduction of phonon scattering at grain boundaries and has a phonon mean free path of up to 775 nm.<sup>31</sup> Moreover, due to the lightness of the carbon atoms, monolayer graphene connected by covalent bonds has an extremely high speed of sound. However, the  $k$  of graphene is anisotropic, and it has a low axial  $k$  because the layers of graphene act through weak van der Waals forces.<sup>32,33</sup>

The  $k$  of graphene can be affected by many factors, including defects,<sup>36,37</sup> number of atomic layers,<sup>34</sup> and size.<sup>38</sup> Various defects such as point defects (vacancies and interstitial atoms), line defects (dislocations), surface defects (grain boundaries and phase interfaces), and bulk defects (cavities and bubbles) are unavoidably present in every crystal (Fig. 1(c)).<sup>39,40</sup> For single-layer graphene, often exhibits point defects and line defects, primarily comprising single-vacancy (SV), Stone-Wales (SW), double-vacancy (DV), and multi-vacancy (MV). Studies of molecular dynamics and non-equilibrium Green's function-based simulation methods have shown that defects tend to reduce the  $k$  of graphene, which is attributed to the fact that the defects lead to scattering of phonons, reducing the mean free path of the phonons.<sup>41–44</sup> Fig. 1(d) shows that the  $k$  of graphene is related to the number of atomic layers, which tends to decrease at room temperature as the number of atomic layers increases.<sup>34</sup> This is due to the different frequencies of phonon vibrations between the different atomic layers, and the inconsistency of the normal modes (different frequencies) of these vibrations creates a “thermal resistance”.<sup>27</sup> The size of graphene is also an influential factor in  $k$ . When the length of graphene is much larger than the phonon mean free path, the  $k$  continues to increase with the graphene length up to a constant value (Fig. 1(e)).<sup>35</sup> Wang *et al.* summarized similar

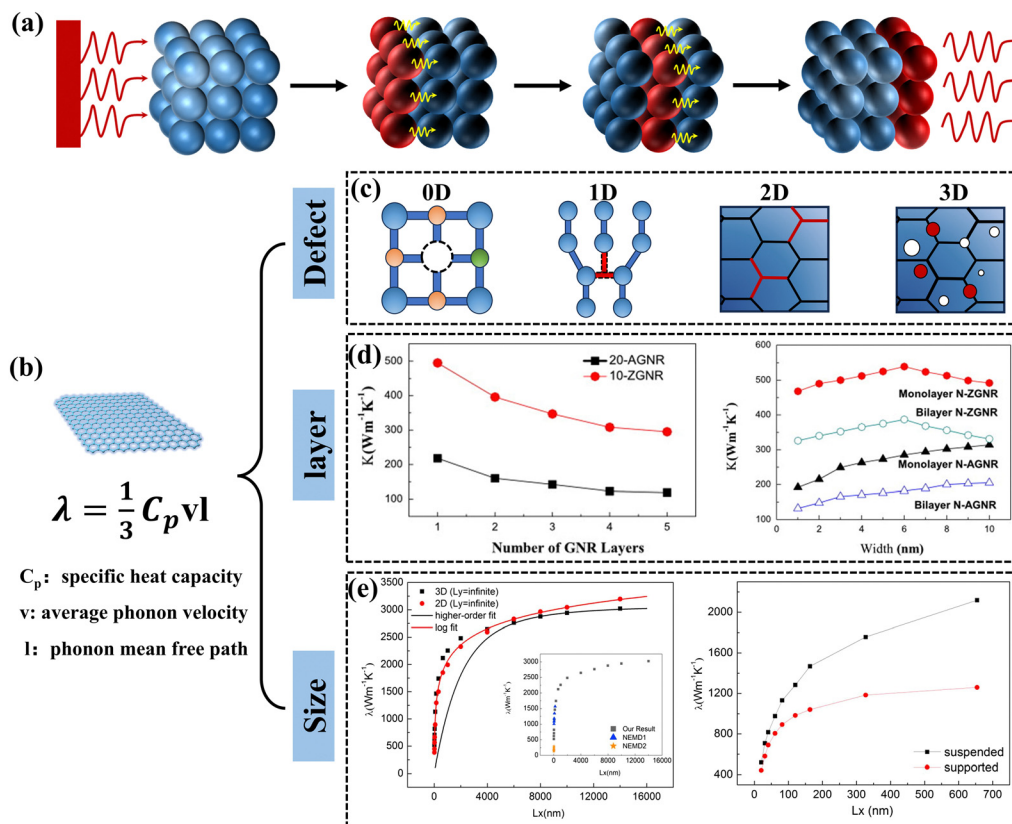


Fig. 1 (a) Schematic diagram of the process by which atoms transfer energy to neighboring atoms through thermal vibrations. (b) Schematic diagram of graphene's special structure. (c) Four defects that affect graphene  $k$ . (d) Layer and size dependence of  $k$  in multilayer graphene nanoribbons (Copyright©2011 Elsevier B.V. All rights reserved).<sup>34</sup> (e) Size effect of  $k$  in monolayer graphene (Copyright©2018 Elsevier Ltd. All rights reserved).<sup>35</sup>

Table 1 The  $k$  and density of different materials

Categorization	Material	$k$ (W m <sup>-1</sup> K <sup>-1</sup> )	Density (g cm <sup>-3</sup> )
Metal	Ag	428	10.4
	Cu	398	8.9
	Au	315	19.3
	Al	247	2.7
	Mg	151	1.7
	Fe	94	7.9
	Ni	88	8.9
Carbon	Graphene	5000	2.3
	Graphite	200–2000 (  )	2.1
		2–800 (⊥)	
	SWCNTs	6000	—
	MWCNTs	3000	—
	PAN-based CF	8–105	1.8
	Pitch-based CF	1100	2.2
Ceramics	Diamond	600–2000	3.5
	BeO	250–300	3.0
	MgO	36	3.6
	Al <sub>2</sub> O <sub>3</sub>	30	3.5
	AlN	170–220	3.3
	SiC	150	3.2
	BN (cubic)	1300	5.2
	BN (hexagonal)	600 (  )	2.1
		30 (⊥)	

conclusions and showed that this result was related to the change in the mode of transport of phonons in graphene.<sup>45</sup> Large-size, defect-free, monolayer graphene is an

ideal thermally conductive filler. However, when graphene is introduced into the polymer matrix, the amorphous polymer chains can severely hinder the heat transfer process of graphene, resulting in the  $k$  of GPNs being much lower than the ideal value. This reveals the complex heat transfer mechanism of GPNs triggers continuous exploration by scholars.

## 2.2 Heat transfer mechanism of GPNs

With the development of electronic products, GPNs have received much attention as thermally conductive materials.<sup>46–48</sup> GPN consists of a polymer matrix and thermally conductive fillers (Fig. 2(a)). The polymer matrix exhibits a low  $k$  due to defects within the polymer chains. Additionally, the intricate spatial structure resulting from the entanglement of these chains can cause significant phonon scattering (Fig. 2(b)).<sup>49</sup> Introducing high  $k$  graphene into polymeric thermally conductive materials is considered to be promising. However, the  $k$  values of polymer composites filled with fillers are much lower than theoretical expectations.<sup>50</sup> Despite high loading, the  $k$  never reaches the intrinsic value of the filler. This is mainly due to the presence of an interfacial thermal resistance (also known as Kapitza thermal resistance) between the polymer matrix and the filler, which impedes the transfer of heat flux (Fig. 2(c)).<sup>51</sup> This interfacial thermal resistance is caused by the phonon vibration

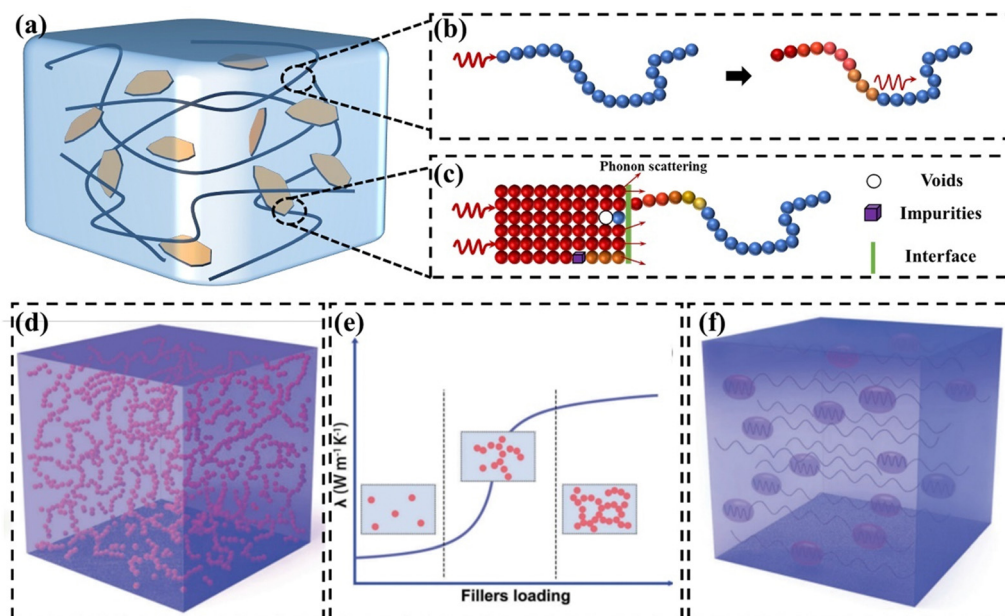


Fig. 2 (a) Representation of a nanocomposite loaded with fillers. (b) Severe phonon scattering is caused by the complex spatial structure formed by the entanglement of polymer chains. (c) Kapitza thermal resistance (d) thermal conduction paths at high filler content (Copyright © 2023 Wiley-VCH GmbH).<sup>21</sup> (e) Thermal percolation theory.<sup>21</sup> (f) Thermoelastic coefficient theory.<sup>21</sup>

mismatch between the polymer matrix and the filler as well as between the filler and the filler.<sup>52,53</sup>

The main mechanisms of heat conduction in GPNs recognized so far are the thermal conduction path theory,<sup>54–56</sup> the thermal percolation theory,<sup>57,58</sup> and the thermoelastic coefficient theory.<sup>21,59</sup> The thermal conduction path theory is the most widely accepted thermal conduction mechanism. When the loading is low, the fillers are isolated and dispersed from each other. Gradually increasing the concentration of fillers, they contact each other in the polymer matrix to form a pathway, which facilitates rapid heat flux transfer (Fig. 2(d)). Thermal penetration theory suggests that there is a process of abrupt change in the  $k$  of polymer composites as the filler content reaches the penetration threshold (Fig. 2(e)).<sup>60</sup> Comparing the polymer matrix to an ocean, the filler is like an island. When the loading of the filler is low, the filler forms a “sea-island” system in the polymer matrix, and they are isolated from each other. As a result, there is no significant improvement in the  $k$  values of the polymer composites. After the loading of the filler reaches the penetration threshold, the  $k$  values of the polymer composites rapidly increase. Nevertheless, some polymer composites do not show significant “heat penetration”.<sup>61</sup> This is difficult to explain by the theory of heat penetration, which is still controversial. Based on the similarity between the vibration law of phonon and the change law of elasticity coefficient in classical vibrational mechanics, some researchers regarded the  $k$  as the thermal elasticity coefficient in the propagation process of phonon and proposed the theory of thermal elasticity coefficient (Fig. 2(f)).<sup>62</sup> The  $k$  depends on the macroscopic properties of the whole material, and the increase in  $k$  of polymer composites can be regarded as the enhancement of the polymer matrix by high fillers.<sup>59</sup> The value

of the  $k$  of the composites gradually increases with the increase in filler content. Polymer matrix and filler are two phases with different thermoelastic coefficients. In the same way that vibrations and waves are reflected, refracted, and interfered at the interface of two phases with different coefficients of elasticity, phonons are also scattered, hindering thermal conduction.

Theoretically, large-sized, defect-free, monolayer graphene is an ideal thermally conductive filler for filling in polymers. However, in polymer composites, the configuration of the filler has a different effect on the  $k$  of the composite due to the interfacial thermal resistance. When the filler loading is low, multilayers of graphene are more favorable to enhance the  $k$ . Shen *et al.*<sup>63</sup> demonstrated through multiscale modeling and experimental methods that multilayer graphene nanosheets with identical aspect ratios consistently enhance the  $k$  of composites more effectively than single-layer nanosheets. This finding is further corroborated by Li *et al.* using molecular dynamics methods.<sup>9</sup> Therefore, substituting multilayer graphene sheets for monolayer sheets represents a more effective strategy for improving the  $k$  of composites.<sup>64,65</sup> However, phonon scattering caused by surface defects is usually the main provider of the total thermal resistance of composites. The interfacial thermal resistance between the polymer and the filler is the key factor affecting its  $k$ .<sup>66</sup> Overall, defect-free and large aspect ratio graphene contributes to the enhancement of the  $k$  of polymer composites, which poses high requirements and challenges for the preparation process of graphene nanosheets.

### 2.3 Modulation of the number of layers and size of graphene

Since the size and number of layers of graphene have a great influence on its thermal properties, the thickness and size of



graphene need to be precisely regulated. Common regulation methods include mechanical exfoliation,<sup>67</sup> epitaxial growth,<sup>68</sup> chemical vapor deposition (CVD),<sup>69</sup> and chemical exfoliation.<sup>70</sup> Mechanical exfoliation is the original method of exfoliating graphite, which is mainly used to overcome the interaction between graphite layers by ultrasound or shear, *etc.* SiC epitaxial growth, a method of preparing single-crystal graphene on a single-crystal substrate, is also considered to be an effective means of producing large-area, high-quality graphene. However, the disadvantages of above two methods are low exfoliation efficiency and uncontrollable thickness and size. CVD is a technique that produces large-area and high-quality continuous graphene films on metal surfaces at high temperatures, allowing for fine control of the number of layers and the size of graphene. Nevertheless, this method is time-consuming and costly and is not conducive to high-volume preparation. In contrast, chemical exfoliation is a promising and effective method for low-cost macro-preparation of graphene. However, most of the prepared graphene is a mixture of monolayer, bilayer and multilayer graphene. All of the above methods used to regulate the number of layers and the size of graphene have their own advantages and disadvantages, and need to be selected according to the actual conditions and demands.

## 2.4 Defect modulation of graphene

Heat conduction in graphene is often greatly hindered by defects, which has driven many scholars to research defect repair. Graphene oxide (GO), with its high yield and ease of preparation, is often used as an alternative to graphene. However, to realize the thermal properties of graphene, it is necessary to repair the functional group defects on GO. The common methods for removing oxygen-containing functional groups from GO are chemical reduction and high-temperature annealing. Chemical reduction is carried out by adding reducing agents such as hydrazine hydrate, alcohols, and sodium borohydride.<sup>71</sup> Zhang *et al.* successfully synthesized reduced graphene oxide (rGO) by reducing GO using hydrazine hydrate (Fig. 3(a)).<sup>72</sup> Xue *et al.* demonstrated that reducing GO with hydrazine hydrate produces rGO with a high carbon-to-oxygen (C/O) ratio. The rGO/polypropylene nanocomposites exhibited significant improvements in tensile strength, thermal conductivity, and thermal stability as the C/O ratio of rGO increased, achieving enhancements of 20.5% in tensile strength and 54.5% in thermal conductivity compared to pure polypropylene.<sup>73</sup> The chemical reduction of GO eliminates various oxygen-containing groups while forming C=C double bonds and partially restoring the conjugated structure of graphene. However, this method faces challenges in completely removing oxygen-containing groups and excess reductants, making high-temperature annealing a practical alternative. Song *et al.* effectively increased the thermal conductivity of GO films to 1043.5 W m<sup>-1</sup> K<sup>-1</sup> through annealing. Higher temperatures (greater than 500 °C) facilitate the removal of functional groups and enhance the conversion of sp<sup>3</sup> to sp<sup>2</sup> carbon in the graphite lattice (Fig. 3(b)).<sup>74</sup> Nevertheless, these methods cannot perfectly enhance the structural integrity of

graphene and new defects may be introduced during the reduction process.<sup>75</sup> Therefore further enhancement of graphene properties requires repair of lattice defects.

The main repair methods for lattice defects in GO include CVD, doping, liquid phase repair, external energy graphitization, and alloying repair. Essentially, lattice defects present in GO can be restored by filling with C radicals or hetero atoms from a C source.<sup>80</sup> For example, Kholmanov *et al.* treated highly oriented pyrolytic graphite using CVD with an acetylene carbon source. Acetylene gas decomposes to supply C atoms for repairing defects. Scanning tunneling microscopy tests revealed that the single-layer depth defects in CVD-treated graphene were repaired, resulting in a perfect honeycomb structure (Fig. 3(c)). But the CVD method makes it difficult to repair multilayer defects.<sup>76</sup> Wang *et al.* demonstrated through first-principles molecular dynamics simulations that vacancies exposed to CO and NO molecules could be healed. CO molecules are trapped in the vacancies, while excess O radicals are removed by NO to form NO<sub>2</sub>. This CO-NO combination effectively facilitates both repair and doping without introducing additional defects (Fig. 3(d)).<sup>77</sup> However, the challenging repair of the polymer matrix and the low efficiency of defect repair restrict the use of graphene as a thermally conductive filler in polymer composites. High-temperature graphitization is a widely used method for repairing lattice defects due to its advantages, which include a straightforward preparation process and high productivity. Xin *et al.* showed that high-temperature treatment at 2850 °C increased the thermal conductivity of graphene flake fibers from 400 W m<sup>-1</sup> K<sup>-1</sup> to 1300 W m<sup>-1</sup> K<sup>-1</sup> by eliminating structural defects, as indicated by the disappearance of the D peak in Raman spectra (Fig. 3(e) and (f)).<sup>78</sup> Liu *et al.* combined high-temperature graphitization of graphene aerogel with vacuum impregnation of EP to create composites with a high *k* of 20.0 W m<sup>-1</sup> K<sup>-1</sup> at 2.30 vol% graphene content, as elevated temperatures removed residual oxygen-containing groups and repaired structural defects (Fig. 3(g) and (h)).<sup>79</sup> Using a similar approach, An *et al.* achieved an exceptionally high *k* of 35.5 W m<sup>-1</sup> K<sup>-1</sup> for graphene-hybridized foam/EP composites with a rGO content of 19.0 vol%.<sup>81</sup>

## 2.5 Surface modification of graphene

Improving the intrinsic *k* of graphene in polymer composites is crucial, but enhancing compatibility between graphene and the polymer matrix is equally important. Increased compatibility reduces phonon vibrational mismatch during heat transfer and improves the dispersion of the filler.<sup>82</sup> Graphene surface functionalization, which includes covalent and non-covalent methods, effectively enhances interfacial compatibility. Covalent bonding introduces functional groups (like -OH, -COOH, -C=O, and -O) that strengthen interfacial bonding energy, thus improving heat transfer efficiency.<sup>83</sup> A study utilizing molecular dynamics simulated the effects of various functionalizations on the interfacial *k* of graphene-EP composites, concluding that covalent bonds enhance interfacial interactions and phonon transfer.<sup>84</sup> However, while creating active

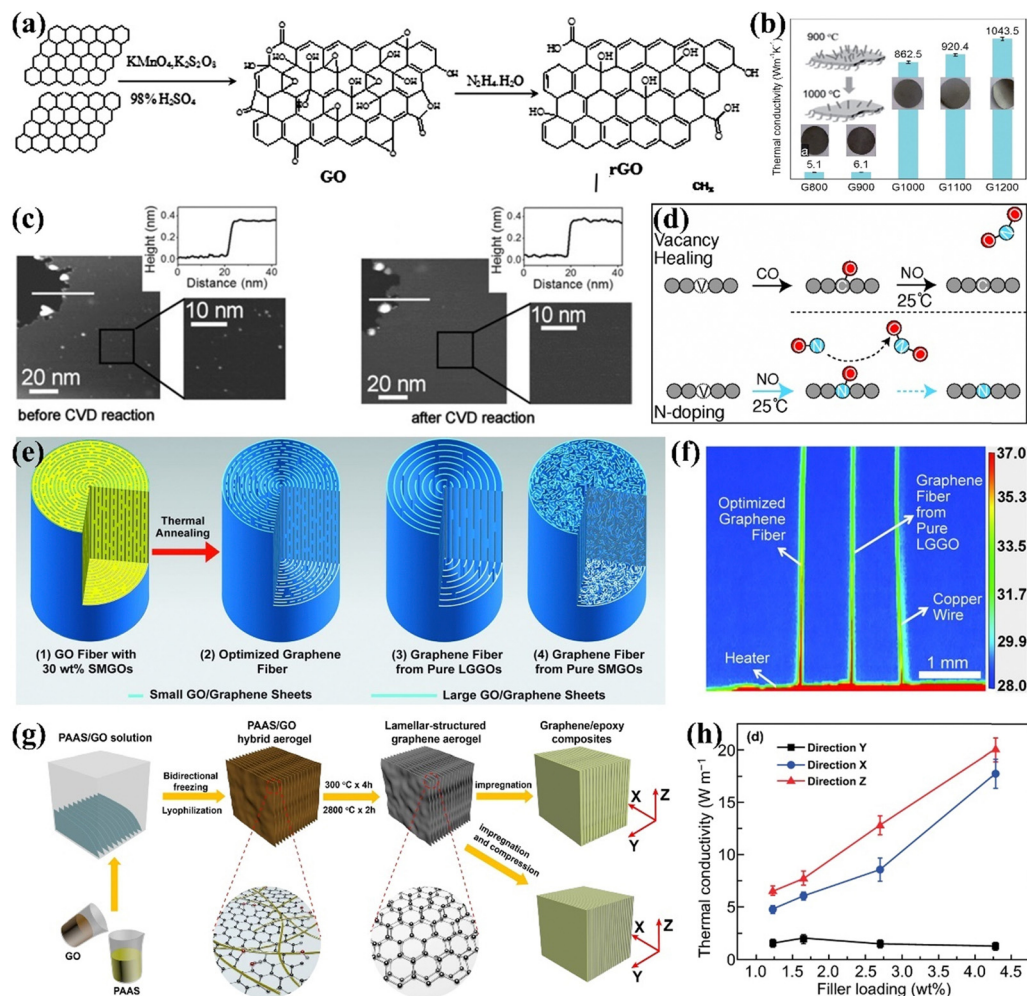


**Fig. 3** (a) The process of reducing GO with hydrazine hydrate (Copyright©2016 Elsevier Ltd. All rights reserved).<sup>72</sup> (b) In-plane  $k$  of rGO films at different annealing temperatures.<sup>74</sup> (c) Repair of single-layer depth defects in highly oriented pyrolytic graphite surfaces by CVD processing (Copyright©2011 Wiley-VCH Verlag GmbH & Co. KGaA, Weinheim).<sup>76</sup> (d) Schematic illustration of the healing and N-doping of graphene vacancies using CO and NO molecules.<sup>77</sup> (e) Schematics of the “intercalated” structure of the GO fibers and graphene fibers, and (f) thermal imaging of fast heat transfer on graphene fibers.<sup>78</sup> (g) Schematic of the fabrication of layered structured graphene aerogels and their EP composites, and (h) plots of the  $k$  of the composites as a function of graphene content in three orientations (Copyright©2020, The Author(s)).<sup>79</sup>

sites for these covalent reactions, the introduction of functional groups can lead to lattice defects, significantly reducing  $k$ , as discussed in Section 2.4. Non-covalent functionalization, increasingly recognized in recent years, utilizes blending or reacting with materials (like surfactants, polymers, organic molecules, and biomolecules) to bridge the gap between graphene and the polymer matrix. This method promotes compatibility through various interactions (ionic, hydrogen bonding,  $\pi$ - $\pi$  interactions, van der Waals forces, electrostatic interactions), without compromising graphene's intrinsic thermal conductivity.<sup>85</sup> Nevertheless, the introduction of non-covalent functional groups introduces impurities that can impact the  $k$  of the composites. Additionally, aligning graphene consistently is challenging due to its dissociative nature. Researchers still have significant opportunities to improve the  $k$  of polymer composites by modulating the interfaces of graphene.

### 3. The structures of graphene in GPNs

Thermally conductive fillers are essential for the performance of GPNs. Initially, graphene was incorporated into the polymer matrix using methods such as solution mixing, *in situ* polymerization, and melt mixing.<sup>86</sup> When graphene is dispersed, the surrounding polymer hinders thermal conduction between the fillers. Therefore, it is essential to increase the filler loading until the percolation threshold is reached to enhance thermal performance by improving contact among the graphene particles. However, a high filler load can lead to clustering due to strong  $\pi$ - $\pi$  interactions, which limits the thermal conductivity of GPNs. Additionally, larger amounts of filler can compromise the flexibility and compressibility of GPNs, hindering their development and application.<sup>87</sup> As the heat flow density in chips increases, traditionally prepared GPNs struggle to meet the demanding heat dissipation requirements of electronic

components. Consequently, researchers are focusing on achieving high  $k$  in GPNs with lower filler loads. Recognized methods to enhance the  $k$  of GPNs include improving the inherent  $k$  of the fillers, creating effective thermal pathways, and reducing interfacial thermal resistance.<sup>16</sup> Since methods to enhance the intrinsic  $k$  of graphene and reduce interfacial thermal resistance were presented in the previous section, this section will summarize strategies specifically related to the construction of effective thermal conductivity pathways.

### 3.1 Hybridization of thermally conductive fillers

The key to enhancing  $k$  by conventional blending methods lies in improving the dispersion of graphene and lowering the thermal percolation threshold of the material. The incorporation of a single filler is limited in improving the  $k$  of polymer composites, mainly owing to the difficulty in uniformly dispersing a single filler and the severe phonon scattering at the interface between the filler and the polymer matrix. The dispersion of fillers in the polymer matrix can be improved by hybridizing multiple fillers into the polymer matrix. The synergistic effect of multiple shapes of fillers helps fillers to construct thermally conductive pathways by bridging and filling the voids, which greatly enhances the heat transfer performance of the composites.<sup>88,89</sup> Graphene nanoparticles (GNPs) are often chosen as a hybridized filler because it has a large aspect ratio, few interfaces, and can form a thermally conductive pathway through face contact. Other fillers with high  $k$  are also frequently used, including 0D fillers (*e.g.*, silicon carbide, diamond, alumina, copper nanoparticles, *etc.*), 1D fillers (*e.g.*, carbon nanotubes (CNTs), carbon nanofibers, silver nanowires, and cellulose nanofibers, *etc.*), and 2D fillers (*e.g.*, boron nitride nanosheets (BNNS), *etc.*). These hybridized thermally conductive fillers have been reported to exhibit synergistic effects in polymer composites.<sup>90,91</sup>

0D fillers require that the size of all three dimensions must be less than 100 nm. When hybridized with 2D graphene nanosheets and incorporated into a polymer matrix, these fillers can effectively fill the voids between the nanosheets. 0D fillers are becoming increasingly prevalent in GPNs because of their ease of production and their ability to enhance the functionality and characterization of the composites. Metal nanoparticles with high  $k$  are often employed to improve the  $k$  of these composites, primarily relying on electron heat transport and exhibiting an extremely short mean-free path. Barani *et al.* incorporated a mixture of fillers, including few-layer graphene (with a size of a few micrometers, 40 wt%) and copper nanoparticles (with a size of a few nanometers, 35 wt%), into EP composites. The resulting  $k$  increased by 6750%, reaching  $13.5 \pm 1.6 \text{ W m}^{-1} \text{ K}^{-1}$ . Copper nanoparticles were positioned between the graphene sheets (Fig. 4(a)), forming a thermally conductive network that combined phonon and electron transport, demonstrating significant potential for TIM.<sup>92</sup> However, due to the excellent electrical conductivity of graphene and metal fillers, GPNs can be challenging to use in electronic devices with high insulation requirements. To harness the exceptional thermal conductivity of graphene while achieving

satisfactory electrical insulation in the composites, a critical strategy is to inhibit electron transfer between neighboring graphene sheets by coating insulating particles on their surfaces. Shen *et al.* successfully grew a layer of  $\text{SiO}_2$  particles on graphene nanosheets using the sol-gel method, resulting in polydimethylsiloxane (PDMS) based composites with excellent thermal conductivity and electrical insulation. This improvement was primarily attributed to the insulating  $\text{SiO}_2$  coating preventing electron transfer between graphene while enhancing inter-component interactions, ensuring uniform dispersion of graphene, and creating an efficient thermal conductivity pathway (Fig. 4(b)).<sup>93</sup> In a study by Lv *et al.*, alumina-coated graphene flakes were utilized to produce EP composites with high  $k$  and low electrical conductivity. A dense  $\text{Al}_2\text{O}_3$  layer formed a mesh structure on the graphene sheet surface, serving as an insulator. The EP composites achieved a  $k$  of  $0.97 \text{ W m}^{-1} \text{ K}^{-1}$  with 30 wt% mixed filler, while electrical resistivity remained above  $10^{11} \Omega \text{ cm}$ .<sup>94</sup>

1D filler is a material characterized by dimensions smaller than 100 nm in at least two directions and demonstrates high  $k$  in one dimension. CNTs are one of the common 1D thermally conductive fillers with  $k$  up to  $1000\text{--}4000 \text{ W m}^{-1} \text{ K}^{-1}$ . Hybridization of CNTs and GNPs can synergistically enhance the  $k$  of GPNs. To fully leverage the anisotropic properties of 1D fillers, CNTs are aligned differently according to the requirements of GPNs. There are three main composite forms of CNTs and graphene, including random distribution (Form 1), horizontal alignment (Form 2), and vertical alignment (Form 3). For the filler random distribution system, CNTs tend to adsorb on the surface of GNPs to form a cross-network (Fig. 4(c)). Compared to the random distribution of a single filler, the incorporation of CNTs usually reduces the restacking of graphene for dispersion, and the CNTs act as bridges connecting the GNPs, which effectively enhances the heat flux transport and uniform distribution.<sup>95</sup> In thin-film GPNs, fillers are often present in a horizontal arrangement. Generally, hybridizing CNTs with graphene enhances the in-plane  $k$  of films. Xiong *et al.* prepared horizontally aligned graphene/CNT films *via* synthesis and compaction. The AB stacking of CNT and graphene facilitated phonon propagation, resulting in an in-plane  $k$  of  $1280.3 \text{ W m}^{-1} \text{ K}^{-1}$  (Fig. 4(d)).<sup>96</sup> However, it is controversial whether the incorporation of CNTs improves the  $k$  of graphene films under Form 2. Xing *et al.*<sup>100</sup> employed molecular dynamics simulation methods and experimental analysis to systematically explore the mechanism of CNTs' influence on the  $k$  of graphene films. It was shown that with the addition of CNTs, the in-plane  $k$  of the hybridized films decreases while the through-plane  $k$  increases, which is mainly due to the increase of defect density by the introduction of CNTs and the creation of covalent bonding between the CNTs and graphene leading to lattice distortion of GNPs, exacerbating the low-frequency phonon scattering. However, the introduction of CNTs provides more channels for phonon transfer in the through-plane direction. Hu *et al.*<sup>101</sup> reported a GO-doped carbon nanotube hybridized film with  $k$  up to  $1056 \text{ W m}^{-1} \text{ K}^{-1}$ . The removal of defects within the film by high-temperature annealing and the



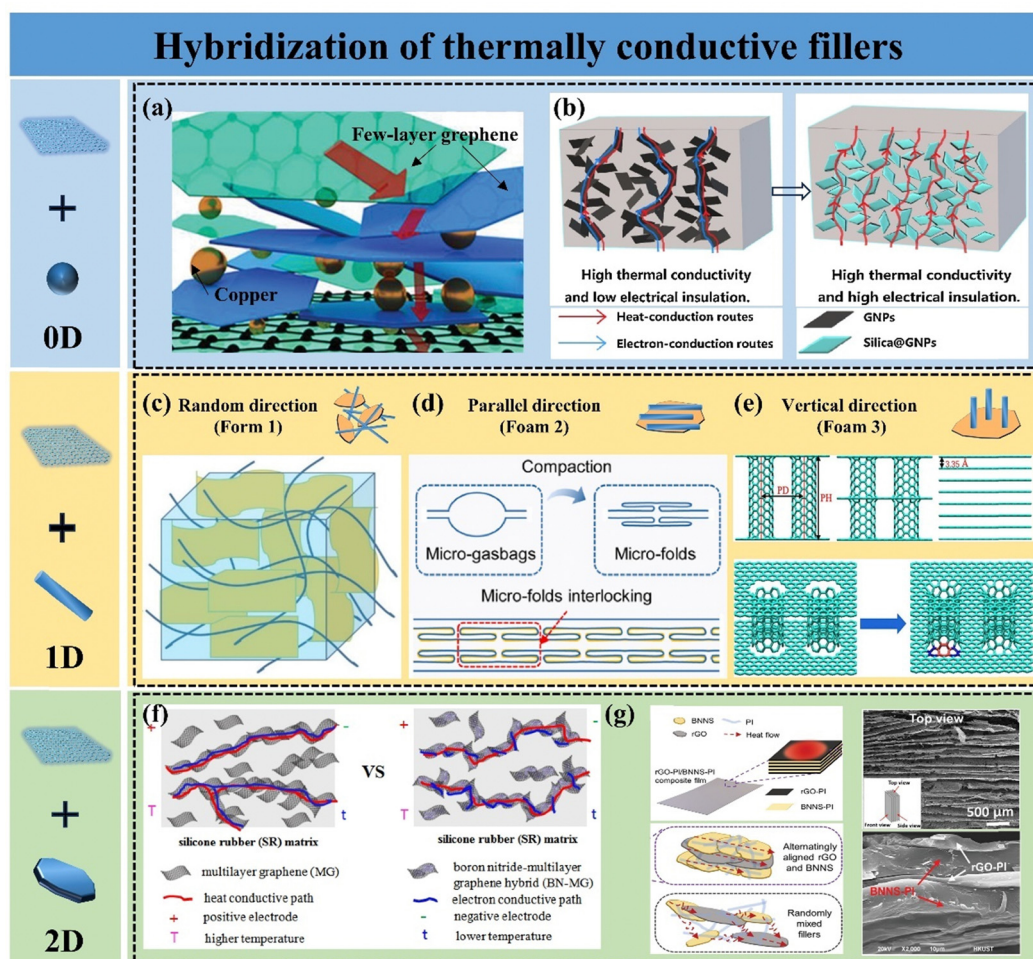


**Fig. 4** (a) Schematic of the formation of thermal conduction pathways by bridging Cu nanoparticles with GNPs (Copyright©2019 Wiley-VCH Verlag GmbH & Co. KGaA, Weinheim).<sup>92</sup> (b) Schematic diagram of the formation of thermal and electrical conduction pathways in silica@GNP/PDMS composites (Copyright©2019, Elsevier).<sup>93</sup> Three composite forms of CNTs and graphene, including (c) random distribution (Copyright©2021 Wiley Periodicals LLC),<sup>95</sup> (d) horizontal orientation (Copyright©2022 Elsevier Ltd and Techna Group S.r.l. All rights reserved),<sup>96</sup> and (e) vertical orientation (Copyright©2023 Elsevier Ltd. All rights reserved).<sup>97</sup> (f) Schematic of the thermal and electrical conduction paths of SR/graphene and SR/BN-graphene composites.<sup>98</sup> (g) SEM images of the rGO/BNNS/PI composite and a schematic illustrating the mechanism behind its high thermal conductivity (Copyright©2020 Wiley-VCH Verlag GmbH & Co. KGaA, Weinheim).<sup>99</sup>

formation of covalent bonds between the CNTs and graphene sheets resulted in the hybridized film having superior properties compared to those prepared by other methods. To improve the  $k$  in the through-plane direction, Georgios K. *et al.*<sup>102</sup> in 2008 reported for the first time a columnar graphene structure consisting of a 1D CNT and a 2D graphene, which corresponds to Form 3. This 3D structure consists of variable-distance parallel graphene layers connected by CNTs placed perpendicularly to the graphene planes. Lin *et al.*<sup>97</sup> demonstrated, using inverse nonequilibrium analytical kinetics (Fig. 4(e)), that carbon nanotube incorporation enhanced the heat transfer between graphene planes but also led to lattice distortion of graphene. Nevertheless, by strategically designing the quantity of CNTs and the number of layers of columnar graphene, the interfacial thermal conductivity between graphene and EP can be significantly enhanced. Regardless of the filler arrangement, the incorporation of CNTs can enhance heat transfer by

efficiently constructing the thermal conduction pathways, but the introduction of crystal defects should be avoided.

Compared to 0D and 1D fillers, 2D fillers can partially substitute for graphene due to their high aspect ratio and similar crystal structure. Hexagonal boron nitride, commonly known as BN, is extensively utilized in the thermal management of electronic devices because of its high thermal conductivity ( $\sim 600 \text{ W m}^{-1} \text{ K}^{-1}$ ), exceptional mechanical properties, favorable thermal stability, and outstanding electrical insulation.<sup>103</sup> The hybridization of boron nitride with graphene not only enhances the thermal transfer performance of GPNs but also imparts new properties to them. According to Deng,<sup>98</sup> the electrostatic self-assembly method was employed to hybridize graphene with BNNSSs, resulting in a silicone rubber (SR)/BNNS-graphene composite that exhibits excellent insulating properties while maintaining high  $k$  (Fig. 4(f)). Feng *et al.* demonstrated that the GPNs produced through the



hybridization of BNNs with graphene also exhibit synergistic effects in flame retardancy.<sup>104</sup> In addition to the inherent properties of BNNs, a well-considered structural design can further enhance the performance of GPNs. Guo *et al.* combined conductive rGO with insulating BN to create PI composites with a high dielectric constant, low dielectric loss, high energy density, and exceptional  $k$ . The micro-sandwich structure facilitates continuous thermal conductivity pathways for both graphene and BNNs (Fig. 4(g)), which synergistically improves the  $k$  of the hybrid filler without compromising its electrical properties. Ultimately, this approach allows for the achievement of performance requirements at significantly lower filler loadings compared to those reported in most studies.<sup>99</sup>

In conclusion, the hybridization of fillers with varying shapes and graphene nanosheets can result in GPNs that possess distinct characteristics. This approach allows GPNs to generally exhibit several advantages, including enhanced performance, diversified functionality, improved dispersion, reduced costs, and optimized interfacial interactions, all of which contribute to their increased utility. However, several challenges remain that require further investigation. For instance, certain types of fillers, such as BNNs and CNTs, are currently difficult to produce in high quality and large quantities.<sup>105</sup> Additionally, GPNs created through simple hybridization methods may not meet the current demands of high heat flow density electronic devices. This limitation arises because simple hybridization does not adequately control the contact configuration between fillers, leading to significant interfacial thermal resistance. Therefore, to minimize microscopic interfacial thermal resistance, it is essential not only to select fillers with complementary properties but also to regulate the bonding state at the filler interface.

### 3.2 3D network alignment of graphene

Simple blending of fillers in polymers can effectively enhance the  $k$  of the material through synergistic effects, but sometimes the enhancement of  $k$  can be affected by the increase of thermal resistance due to the increase of contact area.<sup>106</sup> How to further enhance the  $k$  of polymer composites by reducing the interfacial thermal resistance remains an open question.<sup>107</sup> The combined design of distribution, orientation, and continuity is crucial to achieve the desired thermal properties of the material.<sup>108</sup> The synthesis of continuously oriented graphene structures in polymer matrices is an effective strategy for the development of high-performance polymer composites.<sup>109</sup> Xie *et al.* proposed that the continuity design determined the magnitude of the thermal interactions between reinforcement and matrix, and the control of orientation is a key process to achieve a selective thermal response.<sup>108</sup> Therefore, the construction of thermally conductive pathways can modulate the macroscopic properties of the GPNs. In recent years, there has been an increasing interest in constructing 3D interconnected structures as thermally conductive networks, which ensure good dispersion of low-loaded fillers while minimizing the detrimental effects of interfacial thermal resistance at the filler-filler interface.<sup>22</sup> For example, Li *et al.*<sup>110</sup> constructed a

3D thermal conductivity network of copper and graphene composite, which improved the  $k$  of EP by a factor of 11 owing to the reduction of the filler-filler interfacial thermal resistance. Zhang *et al.*<sup>22</sup> summarized a large number of studies on the preparation methods of dispersed fillers and 3D interconnection networks, and found that composites with 3D interconnection networks were more likely to obtain high  $k$  at relatively low filler fractions. At present, there has been in-depth research on the technologies to construct 3D graphene interconnection networks, mainly including template method, self-assembly method, 3D printing technology and so on.

**3.2.1 Template method.** One popular method for constructing 3D continuous thermally conductive networks is the template method. The primary procedure involves producing a composite material by infiltrating a polymer matrix using a 3D filler skeleton as a template. Numerous studies have focused on creating 3D continuous porous graphene networks through template methods, mainly including the salt template method, bubble template method, Ni template method, and polymer template method. Song *et al.*<sup>111</sup> prepared 3D interconnected graphene networks by the template method with inorganic salt (NaCl), and the composites formed by impregnation into liquid SR. The composite exhibits a high  $k$  of  $1.50 \text{ W m}^{-1} \text{ K}^{-1}$ , achieving a 752% increase with a low graphene loading of 1.46 wt%. (Fig. 5(a) and (b)). This indicates that the 3D interconnected graphene structures prepared by the salt template method have high  $k$  and scalability. Surfactants lower the surface tension of a solution, thereby facilitating the formation of stable bubbles. Li *et al.*<sup>112</sup> incorporated surfactants into a graphene solution to generate bubbles, which were then used to produce foam network graphene/PDMS composites through the bubble template method. This composite exhibited a significant enhancement in thermal conductivity. They used alkyl polyglucoside as a foaming agent, vigorously agitating the GO and GNPs solution to produce a large number of bubbles. Following a chemical reduction reaction and the annealing process, porous graphene foams (GFs) were created with GO and GNP serving as anchors on the bubble surface. The excellent heat conductivity ( $k > 3 \text{ W m}^{-1} \text{ K}^{-1}$ ) and improved EMI shielding of the PDMS composites are made possible by this foam network (Fig. 5(c) and (d)). Numerous studies have demonstrated that both the salt template method and the bubble template method offer advantages such as ease of operation, environmental friendliness, and scalability.<sup>113–115</sup> However, the tight contact between the polymer matrix and the salt nanoparticles can result in curved and meandering porous channels, which necessitate a prolonged duration for the complete removal of the salt templates. For the bubble template method, although template removal is not problematic, it suffers from low thermal conductivity ( $k < 5 \text{ W m}^{-1} \text{ K}^{-1}$ ) due to the presence of curved and tortuous porous channels. Acknowledging that these curved continuous pathways negatively impact heat transfer, researchers have proposed a novel template technique that combines Ni foam with CVD technology. The metallic Ni foam can provide shorter transport pathways, thereby enhancing the  $k$  of GPNs. The CVD

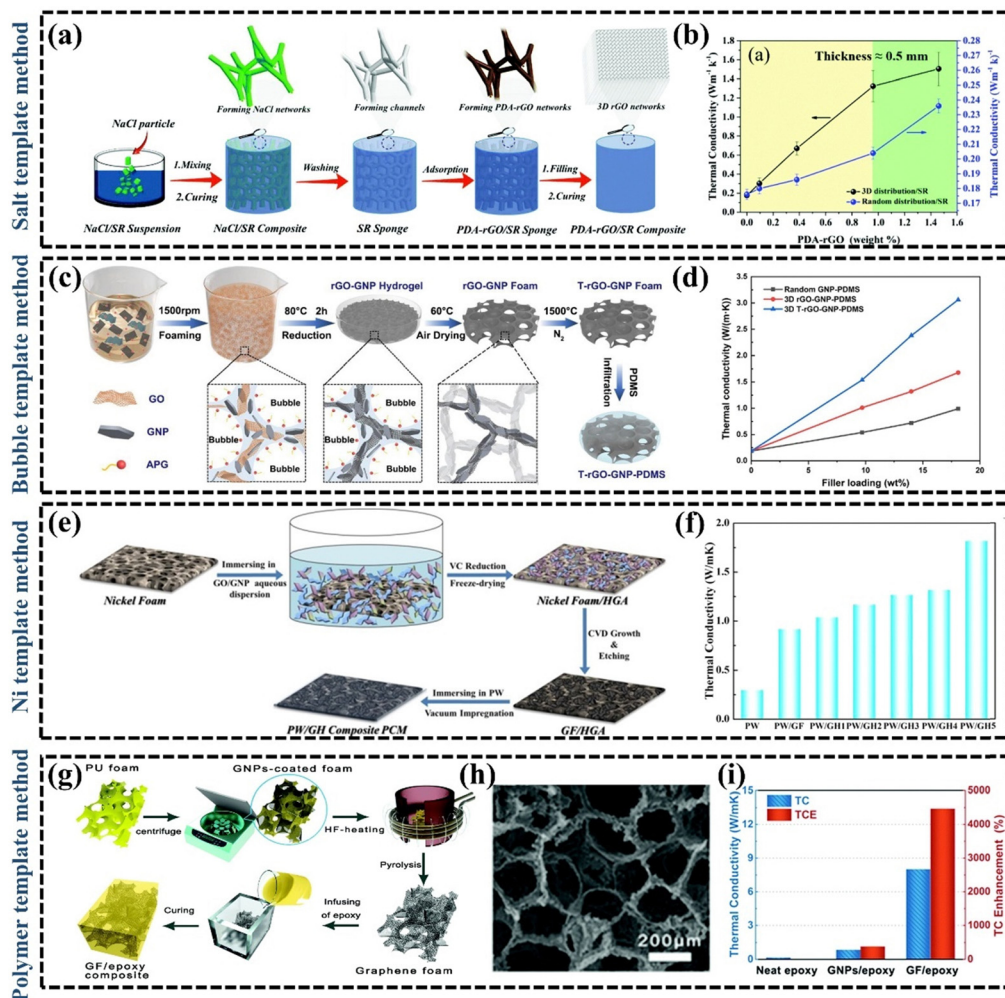


Fig. 5 (a) Schematic illustration of the preparation process of the PDA-rGO/SR composite with 3D interconnected graphene networks (Copyright©2021 Elsevier B.V. All rights reserved).<sup>111</sup> (b) The TCs of PDA-rGO/SR composites.<sup>111</sup> (c) Schematic illustration of the fabrication procedure of 3D rGO-GNP-PDMS composites (Copyright©2021 Elsevier B.V. All rights reserved).<sup>112</sup> (d) Effect of the GNP content on the  $k$  values of random GNP-PDMS, 3D rGO-GNP-PDMS, and 3D T-rGO-GNP-PDMS composites.<sup>112</sup> (e) Schematic illustration of the preparation of GO/GNP/PW composites (Copyright©2017 Published by Elsevier B.V.).<sup>118</sup> (f) The  $k$  of pure PW, and PW composites.<sup>118</sup> (g) Preparation process of graphene foam/EP composites.<sup>120</sup> (h) SEM image of graphene foam.<sup>120</sup> (i) The  $k$  of graphene foam/EP composites.<sup>120</sup>

method is widely considered a reliable technique for producing high-quality graphene with few defects and high  $k$ .<sup>116</sup> Therefore, the nickel template method, when used in conjunction with CVD technology, can enhance the  $k$  of composites by creating high-quality 3D pathways. Chen *et al.*<sup>117</sup> fabricated a layer of graphene on a nickel foam *via* CVD, then removed the nickel using acid to obtain a graphene skeleton. Yang *et al.* vacuum-impregnated the graphene skeleton with paraffin wax (PW). The  $k$  of the composite phase change material was enhanced by 574% compared to pure PW (Fig. 5(e) and (f)).<sup>118</sup> Although this method is effective in enhancing the  $k$  of composites, CVD method is regarded as one of the most unfavorable methods for scalable preparation due to its complexity, high cost and time-consuming.<sup>119</sup> The polymer template method has been utilized more extensively than the Ni foam template method because it is not only straightforward to

operate but also creates a continuous pathway for improved  $k$ . Polymer sponges, including melamine sponges, PU sponges, and PI sponges, are commonly employed as natural 3D soft templates. These templates are commonly used to create continuous interconnecting networks of fillers because of the method's convenience. Liu *et al.*<sup>120</sup> developed composites by coating PU templates with GNPs, and then encapsulating them in EP. The  $k$  of the polymer composites reached  $8.04 \text{ W m}^{-1} \text{K}^{-1}$ , marking a significant 4473% increase compared to the polymer matrix when the graphene content reached 6.8 wt% (Fig. 5(g)–(i)). Despite the high  $k$  achieved at low filler loadings, the polymer template method presents several challenges in its application. Generally, polymers decompose into toxic substances during the heat treatment process, which poses risks to human safety.<sup>121</sup> Additionally, the graphene attachment process in the polymer template method is typically conducted

in the liquid phase, resulting in uneven dispersion of fillers. Consequently, the polymer template method faces difficulties in large-scale production.

**3.2.2 Self-assembly method.** The self-assembly method is simpler than the template method because it does not require auxiliary templates to create a thermally conductive network. This approach involves allowing GO to spontaneously aggregate into a continuous 3D network during the reduction process. Subsequently, solvent removal is achieved through cooling and drying or supercritical drying, resulting in the production of graphene aerogels. Finally, a polymer matrix is infused into the aerogel and cured to create GPNs.<sup>122</sup> GO and rGO are considered attractive building blocks for “bottom-up” self-assembly due to various non-covalent forces such as hydrogen bonding, van der Waals interactions,  $\pi$ - $\pi$  interactions, and hydrophobic-hydrophilic interactions.<sup>123</sup> The preparation of graphene aerogels through GO self-assembly methods (including hydrothermal reduction, chemical reduction, *etc.*) offers a simple approach to creating 3D thermally conductive networks.<sup>124,125</sup> The hydrothermal self-assembly method is not only simple but also reduces the interfacial thermal resistance of GPNs due to the effective interaction and dispersion of GO. Feng *et al.*<sup>104</sup> fabricated a 3D rGO@Ni(OH) framework using a two-step hydrothermal method. The framework was composited with BN and EP to obtain a ternary composite. In the ternary composites, this framework not only prevents the stacking but also connects neighboring BNNSS. The composites prepared using this method exhibit a high  $k$  of  $2.01 \text{ W m}^{-1} \text{ K}^{-1}$ , and the synergistic effect is enhanced by 39.4% compared to EP/BN composites (Fig. 6(a) and (b)). The chemical reduction approach is more frequently used for graphene self-assembly than the hydrothermal method due to lower reaction temperature. Liang *et al.*<sup>48</sup> developed a 3D heterostructure material comprising reduced rGO-BN by stacking BNNSS onto the surface with a silicone grease binder, utilizing rGO as the substrate. Due to the incorporation of graphene and its phonon-matching structural properties, the 3D rGO-BN exhibited enhanced  $k$  in silicone grease compared to BNNSS (Fig. 6(c) and (d)). Despite the relative simplicity and maturity of self-assembly methods, achieving large-scale continuous production remains a significant challenge. Additionally, because the fillers are self-assembled through weak interactions, GPNs may experience low mechanical strength and difficulties in regulating porosity.

**3.2.3 3D printing technology.** The emerging 3D printing technology can form structures precisely from microscopic to macroscopic scales, as opposed to the difficult-to-control microscopic scale 3D interconnected thermally conductive network structures prepared by self-assembly and template methods. 3D printing technology allows the preparation of graphene structures with the same structure on different scales when graphene is used as a model precursor.<sup>127</sup> The precise tuning of this technique is of great interest for the preparation of thermal pathways as it is not limited by structural complexity. As the polymer composite melt passes through the fine nozzle, the fillers form oriented structures overlapping each other. The

oriented stacking of fillers facilitates the formation of continuous pathways, thereby enhancing the  $k$  of the polymer composite. However, traditional 3D printing technologies struggle to process elastomeric materials, significantly limiting the application of 3D printing in thermal conductivity and heat dissipation. To address this issue, Lv<sup>126</sup> and colleagues selected polyolefin elastomer for its excellent processability and high elasticity as the matrix, and GNPs as the filler for thermal conductivity and reinforcement. Functional filaments with a network structure of GNPs were prepared using ultrasonic mixing and a single-screw extruder. The morphology of these filaments is advantageous for processing and molding GNPs/polyolefin elastomer composites into various shapes. The multifunctionality, high elasticity, and effective heat dissipation properties (with a thermal conductivity of  $4.3 \text{ W m}^{-1} \text{ K}^{-1}$  at 10.93 vol% filler loading) of the printed components can be achieved by optimizing the porous structure (Fig. 6(e) and (f)). Although this method can establish a continuous thermal conductivity pathway, the contact thermal resistance between the filler and the matrix significantly hinders the heat dissipation of the composite. It has been suggested that this challenge can be mitigated through filler hybridization. Introducing BN to create a secondary network is a promising strategy, as it not only synergistically enhances the  $k$  of GNPs but also preserves their excellent electrical insulation properties.<sup>128,129</sup> However, 3D printing necessitates the use of expensive equipment and is highly selective regarding the polymer matrix, which greatly restricts the industrial scalability of this method.<sup>130</sup>

### 3.3 Horizontal alignment of graphene

Besides the method of 3D interconnecting thermally conductive pathways, aligning thermally conductive fillers can enhance heat transfer in specific orientations. The perfect orientation of 2D graphene can maximize its excellent in-plane properties and lower the percolation threshold of the material. A crucial strategy for creating highly anisotropic thermally conductive nanocomposites involves aligning the fillers along the in-plane direction within the polymer matrix. This enables the establishment of horizontal thermal conductivity pathways, thereby maximizing the in-plane  $k$ .

**3.3.1 Vacuum filtration-assisted assembly and layer-by-layer self-assembly (LBL).** The vacuum filtration-assisted assembly is a simple and effective technique for aligning graphene. With the help of a vacuum system, graphene dispersed in solution is aligned by a filter membrane under suction, resulting in the formation of a dense, horizontally aligned structure. Therefore, this method is particularly suitable for the preparation of GPNs in paper or sheet form. It is commonly employed in numerous studies due to its operational simplicity and low costs. To achieve high  $k$ , researchers have primarily concentrated on optimizing the functionalization and size of the fillers, as well as hybridizing different types of fillers. The mismatch in surface tension between graphene ( $46.7 \text{ mJ m}^{-2}$ ) and water ( $72.75 \text{ mJ m}^{-2}$ ) resulted in sample cracking during filtration. Consequently, researchers incorporated surfactants into the graphene suspension to enhance the



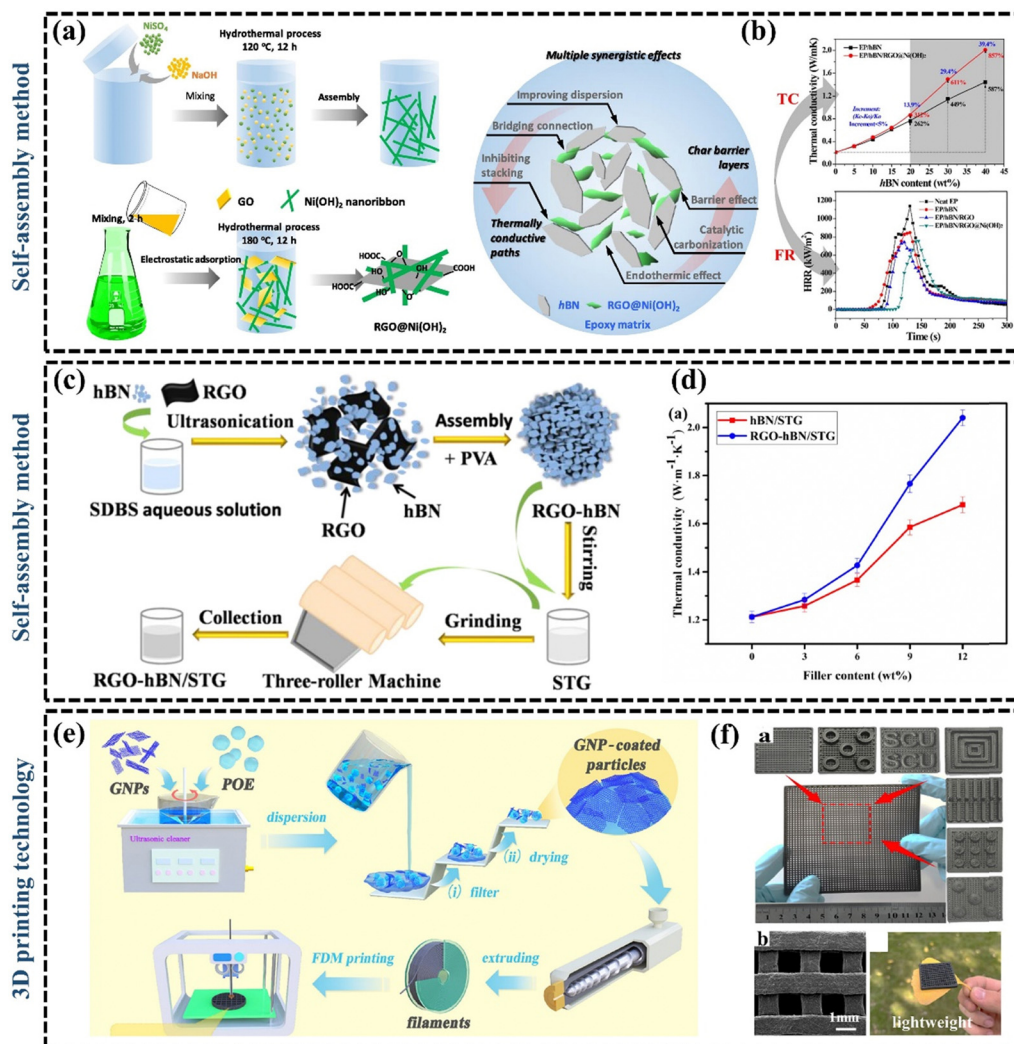


**Fig. 6** (a) Illustrations of synthesis routes of  $\text{rGO@Ni(OH)}_2$  hybrid by “two-step” hydrothermal process and multiple synergistic effects of BN and  $\text{rGO@Ni(OH)}_2$  hybrid in EP matrix (Copyright©2019 Elsevier B.V. All rights reserved).<sup>104</sup> (b) The  $k$  of EP/BN and EP/BN/ $\text{rGO@Ni(OH)}_2$  composites as a function of BN content and heat release rate of neat EP and its composites with 20 wt% BN and 2 wt% graphene.<sup>104</sup> (c) Scheme for the preparation of RGO-BN/silicone thermal grease (Copyright©2022, American Chemical Society).<sup>48</sup> (d) The  $k$  of BN/silicone thermal grease and RGO-BN/silicone thermal grease with different filler contents.<sup>48</sup> (e) Schematic diagram for preparation of polyolefin elastomer/GNP filaments and the 3D printing process (Copyright©2022, American Chemical Society).<sup>126</sup> (f) SEM images, ultra-depth images, and digital photos of printed flexible polyolefin elastomer/GNP pads.<sup>126</sup>

dispersion of graphene. Using the improved method, graphene frameworks with a thickness of up to 3 cm and a density of  $120\text{--}150\text{ mg cm}^{-3}$  were produced. When embedded in an EP containing 13.6 wt% graphene, the framework imparted an in-plane  $k$  of up to  $12.4\text{ W m}^{-1}\text{ K}^{-1}$  to the composite. Although this method effectively reduces graphene aggregation, it still encounters challenges related to product inhomogeneity in large-scale samples.<sup>131</sup> To further improve the dispersion of fillers and the  $k$  of GPNs, many studies have opted to incorporate additional fillers for hybridization. He *et al.*<sup>132</sup> prepared a unique hierarchical structure using the vacuum filtration-assisted assembly method (Fig. 7(a)–(c)). They utilized aramid nanofibers with high specific surface area and specific strength as polymer matrices and incorporated graphene nanosheets and CNTs to fabricate nanocomposites. The material has a

unique hierarchical structure that can create thermal conductive networks in the in-plane direction, resulting in an in-plane  $k$  as high as  $20.54\text{ W m}^{-1}\text{ K}^{-1}$  with just 20 wt% of graphene loading. Despite the simplicity and low cost of this method, the filtration rate requirement is high. An excessively fast rate prevents the filler from orienting properly, thereby compromising the quality of the GPN. Conversely, a rate that is too slow can negatively impact production efficiency. LBL technology is a method for creating multilayer composite films or hierarchical nanostructures from the bottom up. By adjusting interaction forces like hydrogen bonding, covalent bonding, and charge interactions between different nanolayers, self-assembly can be achieved. Studies have shown that this method offers more precise control compared to vacuum-assisted self-assembly (Fig. 7(d)–(g)).<sup>133</sup>



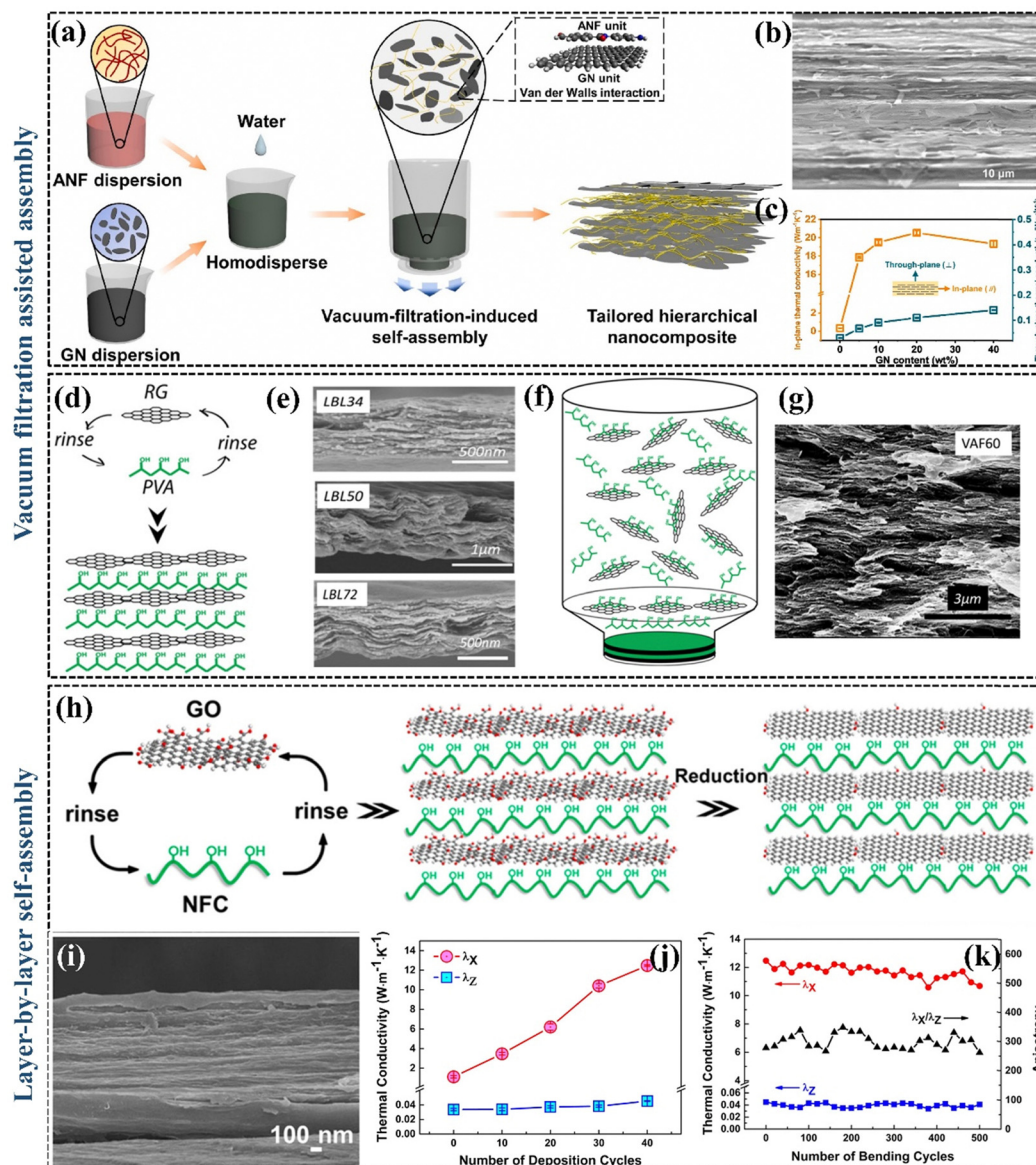


Fig. 7 (a) Schematic illustration of the preparation process of aramid nanofibers/GNP nanocomposites (Copyright©2022 Elsevier Ltd. All rights reserved).<sup>132</sup> (b) SEM image of aramid nanofibers/20% GNP nanocomposite film.<sup>132</sup> (c) In-plane and out-plane  $k$  of aramid nanofibers nanocomposite films prepared with different GNP contents.<sup>132</sup> (d) A schematic drawing of LBL assembly (Copyright©2013, American Chemical Society).<sup>133</sup> (e) SEM images for the cross-sectional areas of LBL34, LBL50, and LBL72. (f) A schematic drawing of vacuum filtration-assisted assembly.<sup>133</sup> (g) SEM image for the cross-sectional areas of vacuum filtration-assisted 60.<sup>133</sup> (h) Schematic drawing of the preparation of the hybrid films (Copyright©2017, American Chemical Society).<sup>135</sup> (i) The cross-section of the thermally conductive coating layer.<sup>135</sup> (j)  $k_X$  and  $k_Z$  of LBL-assembled (nanofibrillated cellulose/rGO)<sub>n</sub> hybrid film with different numbers of deposited cycles on a nanofibrillated cellulose substrate.<sup>135</sup> (k)  $k_X$ ,  $k_Z$ , and  $k_X/k_Z$  of (nanofibrillated cellulose/rGO)<sub>40</sub> hybrid film under different numbers of bending cycles.<sup>135</sup>

Consequently, there is a wealth of research on using the LBL method for making GO/polymer composite films. Techniques for preparation include dip-assisted, spin-assisted, and spray-assisted self-assembly. For instance, Song *et al.*<sup>134</sup> employed a spin-assisted LBL process to produce an SR/graphene film with excellent  $k$ . This structured film enhanced heat transfer with a  $k$  of  $2.03 W m^{-1} K^{-1}$ . To expand thermal management applications in flexible materials, Song *et al.* developed a method of self-assembling GO onto flexible nanocellulose layer by layer using hydrogen

bonding. This innovative approach streamlined the deposition process and created a hierarchical structure, boosting the material's  $k$  to  $279 W m^{-1} K^{-1}$ , which is far superior to traditional polymer-based nanocomposites (Fig. 7(h)–(k)).<sup>135</sup> As with vacuum-assisted self-assembly methods, samples prepared using LBL techniques may experience layer-to-layer inhomogeneity during large-scale production. Additionally, this method may result in insufficient mechanical strength of the material, as the bonding between layers primarily relies on physical or chemical interactions.

**3.3.2 Solvent evaporation and hot compression.** Compared to the vacuum filtration-assisted assembly method and the LBL self-assembly method, the solvent evaporation and hot compressing techniques represent a significant advancement in large-scale preparation and the mechanical properties of the GPNs. Inspired by the unique pearl layer structure of natural shells, a series of research on biomimetic nanocomposites have been reported. Nanocomposites consisting of alternating regular arrangements of nanofillers, and polymer matrices have been shown to have excellent toughness and  $k$ . This is attributed to the pearl layer connection that effectively reduces thermal resistance and transports heat efficiently. However, most of the methods for preparing pearl layer structures are not simple, fast, and easy to scale up, which greatly limits their applications. In contrast, solvent evaporation-induced self-assembly is a simple, efficient, and large-scale self-assembly process by evaporation of solvents. Li *et al.* prepared large-area

bulk polypropylene carbonate propylene/poly(tetrahydrofuran)-functionalized reduced GO nanocomposites with pearl-laminated structures. The introduced interconnected channels of the pearl layer structure significantly improved the thermal, mechanical, and shape memory properties of the composites, and the resulting nanocomposites had out-plant  $k$  as high as  $25.7 \text{ W m}^{-1} \text{ K}^{-1}$ .<sup>136</sup> To further enhance the in-plane thermal conductivity and mechanical properties, Zou *et al.* established robust interactions by introducing covalent bonds. They prepared strongly covalently bonded cross-linked graphene-graphitized polydopamine-carbon nanotube composite films through evaporative self-assembly, chemical reduction, carbonization, graphitization, and mechanical compaction. The unique structure of the composite film facilitated load transfer and energy dissipation between the components, which greatly improved the  $k$  of the composite film (Fig. 8(a)–(c)).<sup>137</sup> Although the in-plane thermal conductivity is enhanced,

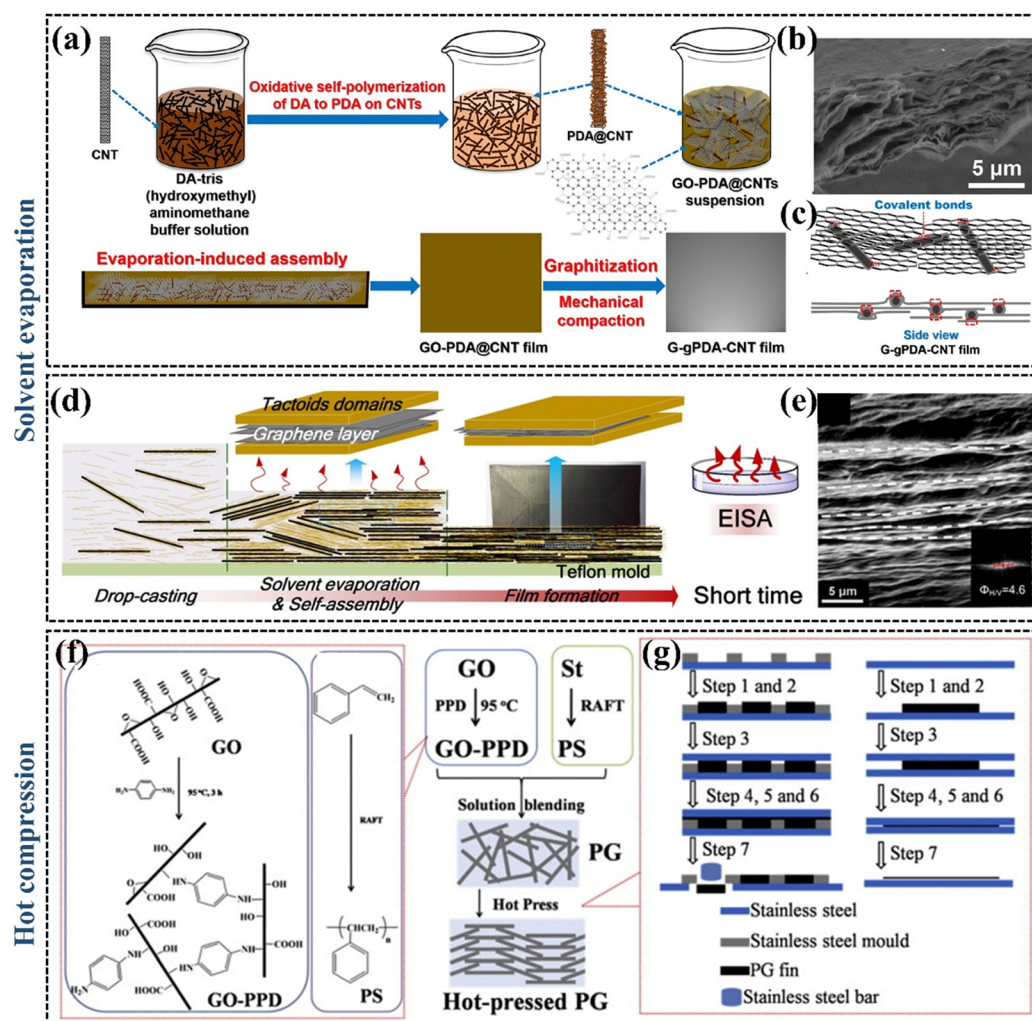


**Fig. 8** (a) The preparation process of the G-gPDA-CNT films (Copyright©2020, American Chemical Society).<sup>137</sup> (b) SEM image showing the microstructure of the cross-section of G-gPDA-CNT-7.5% film (Copyright©2018, American Chemical Society).<sup>137</sup> (c) Mechanism of the G-gPDA-CNT-7.5% film (Copyright©2018, American Chemical Society).<sup>137</sup> (d) Schematic representation of the vacuum filtration-assisted assembly and solvent evaporation fabrication of rGO/oxidized cellulose nanocrystal nanocomposites (Copyright©2018, American Chemical Society).<sup>139</sup> (e) SEM image of rGO/oxidized cellulose nanocrystal nanocomposites.<sup>139</sup> (f) and (g) The preparation of hot-pressed PG thermal conductive fins (Copyright©2015 Elsevier Ltd. All rights reserved).<sup>140</sup>

solvent-dispersible nanofillers are prone to agglomeration due to the increased concentration during solvent evaporation. Zeng *et al.* demonstrated that the addition of oxidized cellulose nanocrystals to a mixture solution of GO and graphene can effectively address the issue of filler agglomeration. Oxidized cellulose nanocrystals not only serve as dispersants for various water-dispersible nanomaterials but also spontaneously self-assemble with the target nanomaterials into long-range aligned structures through an evaporation-induced self-assembly process.<sup>138</sup> They formed interference-free self-assembled long-range aligned nanocomposites with graphene by evaporation-induced self-assembly technique based on the excellent dispersibility of cellulose nanocrystals. Compared to conventional polymer composites, the material achieves more than one order of magnitude higher  $k$  with only 4.1 vol% graphene due to the long-range ordered structure and strong intermolecular forces (Fig. 8(d) and (e)).<sup>139</sup> The solvent evaporation method, while easily performed at room temperature, exhibits low productivity due to the extended time required for complete solvent evaporation. Additionally, any residual solvent may adversely affect the material properties, necessitating strict control over the type of solvent used and the evaporation conditions. The hot compression technique is used for cost-effective large-scale manufacturing. It improves the filler's alignment by applying pressure in heated conditions. In general, this method is used to support other alignment strategies. Wang *et al.* created robust cellulose-based nanocomposites through aqueous solution evaporation and hot compression. Ding *et al.* developed polystyrene/graphene composites using solution mixing and hot compression. The  $k$  of composites with 10 wt% graphene increased by 66% compared to pure polystyrene due to the anisotropic arrangement of hot-pressed graphene (Fig. 8(f) and (g)).<sup>140</sup> The results indicate that hot compression enhances the contact between the filler and the matrix, potentially increasing the density of the filler and leading to a rapid and efficient improvement in the  $k$  of the GPNs. However, elevated temperatures and pressures may decompose temperature-sensitive polymers, significantly limiting the range of polymers that can be utilized. Additionally, hot compression requires the use of molds, which increases equipment investment and operational costs, presenting a challenge for the Industrial production.

### 3.4 Vertical alignment of graphene

To achieve effective through-plane heat transfer in GPN materials, researchers created vertically aligned 3D graphene structures that leverage graphene's superior in-plane thermal conductivity and various methods to integrate them with polymer matrices. Lin *et al.*<sup>141</sup> prepared four TIM (pristine PDMS/ randomly dispersed graphene-based PDMS composites/ horizontally oriented graphene backbone PDMS composites/ axially oriented graphene backbone PDMS composites) by freeze-drying and vacuum impregnation. By comparing their  $k$ , it was found that graphene backbone PDMS composites with vertical orientation had a significant improvement. The reason is that vertically oriented graphene networks can provide

shorter transmission paths and enhance the transmission rate, for which a great deal of effort has been made in constructing vertically aligned graphene networks to form fast heat transfer channels.

**3.4.1 External fields assisted alignment.** The applied external fields not only remotely modulate graphene but also offer flexible orientation selectivity, which is excellent for the preparation of vertically aligned GPN.<sup>142</sup> The three main approaches currently reported to achieve graphene alignment based on field-filler interactions mainly include flow-field-induced alignment, electric-field-induced alignment, and magnetic-field-induced alignment. Flow-field-induced techniques, although widely used in polymer processing, are primarily limited to unidirectional orientation along the flow direction and are also constrained by sample size limitations.<sup>143</sup> Furthermore, highly viscous-filled polymers experience alignment gradients due to variations in shear and tensile rates during flow.<sup>144</sup> These factors significantly impede the advancement of flow-induced techniques. By applying an electric field, the conductive filler will form a linear bundle pulled by the electric field force. The control of the conductive path can be effectively realized by changing the power supply as well as the power supply parameters.<sup>145,146</sup> Park *et al.* prepared vertically aligned graphene/PDMS composites under different electric fields. By comparing the application of both direct current and switched direct current electric fields, the experimental results indicate that the electric field generated by the switched direct current enhances the  $k$  of vertically oriented GNP by more than 112% (Fig. 9(a)–(c)). The increased viscosity of the substrate necessitates a higher voltage between the electrodes to orient the electric field of numerous nanoparticles. However, this elevated voltage poses a risk of electrical breakdown of the material. To mitigate this risk, they coated the electrodes with an insulating layer to prevent electrical sparking under the applied current.<sup>147</sup> In addition to the challenge of electrical breakdown, the electric field-assisted orientation approach has some other limitations. For example, the effect of pH and charge. Due to the limitations of flow and electric fields, magnetic field-induced alignment has emerged as the most appealing and easily manipulable technique for aligning fillers. Additionally, magnetic fields offer a homogeneous, flexible, non-contact, and scalable method for aligning graphene nanosheets. He *et al.* demonstrated that the magnetic field-induced perpendicular alignment of graphene can significantly enhance the thermal conductivity of polymers, even with reduced filler loading levels. This presents substantial potential for thermal management applications to address various technological demands. They endowed multilayer graphene with magnetic properties by coating its surface with iron oxide nanoparticles. Under the action of a strong magnetic field, the graphene is vertically oriented, which leads to an increase in  $k$  of the EP composite by 311.6% (Fig. 9(d)–(g)). High  $k$  ( $0.708 \text{ W m}^{-1} \text{ K}^{-1}$ ) was achieved at an ultra-low graphene loading level (3.36 wt%).<sup>148</sup> Geng *et al.* also demonstrated that magnetically induced vertical alignment of graphene significantly enhances the thermal conductivity of polymers. They prepared rGO@Fe<sub>3</sub>O<sub>4</sub>/EP composites by



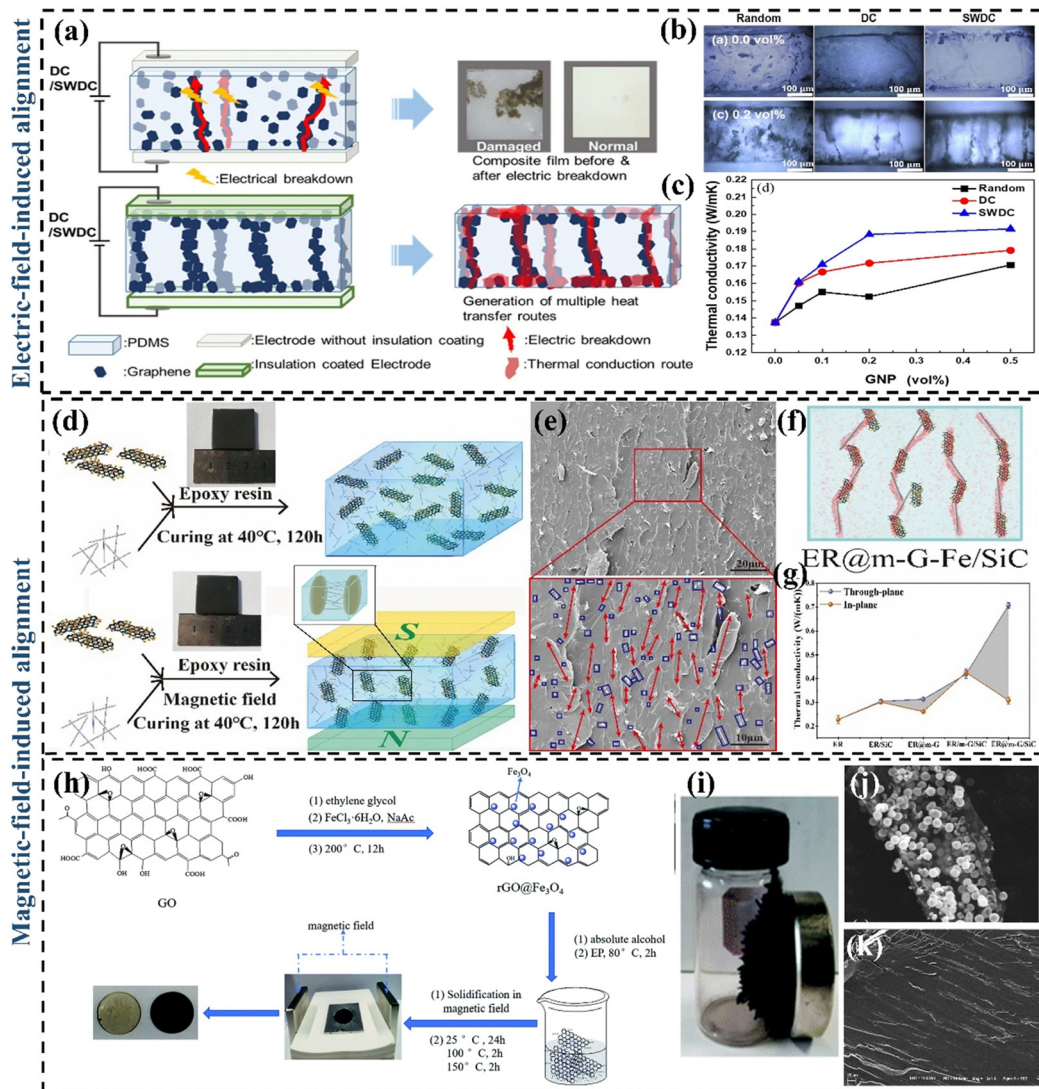


Fig. 9 (a) Mechanism diagram of the electric field-induced alignment of graphene (Copyright©2021 Elsevier B.V. All rights reserved).<sup>147</sup> (b) Cross-sectional digital micrographs of PDMS/GNP composites with 0.1 vol% and 0.5 vol% prepared using different electric fields (Copyright©2021 Elsevier B.V. All rights reserved).<sup>147</sup> (c) The  $k$  of PDMS/GNP composites as a function of GNP content (Copyright©2021 Elsevier B.V. All rights reserved).<sup>147</sup> (d) Preparation process of ER/m-graphene-Fe/SiC composites with external magnetic field (Copyright©2020 Published by Elsevier Ltd).<sup>148</sup> (e) The cross-sectional SEM images of ER@m-graphene-Fe/SiC-3.36 wt% (the red arrows represent the m-G-Fe in ER composites; the blue circles represent the dispersion of SiC nanowires).<sup>148</sup> (f) Schematic diagram of the cross-section of the through-surface  $k$  of the ER@m-graphene-Fe/SiC composite material.<sup>148</sup> (g) The comparison of through-plane  $k$  and in-plane  $k$  of ER composites.<sup>148</sup> (h) Synthesis of rGO@Fe<sub>3</sub>O<sub>4</sub> and preparation of rGO@Fe<sub>3</sub>O<sub>4</sub>/EP.<sup>149</sup> (i) Image of rGO@Fe<sub>3</sub>O<sub>4</sub>.<sup>149</sup> (j) SEM images of rGO@Fe<sub>3</sub>O<sub>4</sub> nanocomposite. (k) Cross-sectional SEM image of rGO@Fe<sub>3</sub>O<sub>4</sub>/EP parallel to the magnetic field direction.<sup>149</sup>

solvothermal method. It was shown that rGO@Fe<sub>3</sub>O<sub>4</sub> was uniformly dispersed in the EP and aligned along the magnetic field direction. Compared with the pure EP, the  $k$  parallel to the magnetic field direction was enhanced by 196.6% (Fig. 9(h)–(k)).<sup>149</sup> However, due to the antimagnetic of graphene and polymer matrix, the strength of the magnetic field is often required to be high. This presents a challenge for large-scale preparation.

**3.4.2 Ice-template.** The ice template method, known as freeze casting, is a bottom-up approach for producing porous materials with bionic structure and adaptability. Initially, ice crystals are aligned vertically by extruding and trapping fillers during growth, and then the ice templates are removed through

freeze-drying, resulting in long-range aligned 3D skeletons. This method has demonstrated its flexibility, scalability, and versatility compared to other techniques.<sup>150</sup> Researchers have successfully controlled the structure formation by manipulating the temperature field. Different freezing directions (homogeneous, unidirectional, and bidirectional freezing) lead to various porous structures (isotropic, cellular, and long-range lamellar structures).<sup>151</sup> Jin *et al.* investigated the impact of various temperature gradients on the alignment of 3D microstructures of fillers. They fabricated MXene/graphene aerogels and vacuum-infused polyethylene glycol (PEG) to produce PFG/MXene/graphene composites through both unidirectional and bidirectional freezing techniques. The experimental



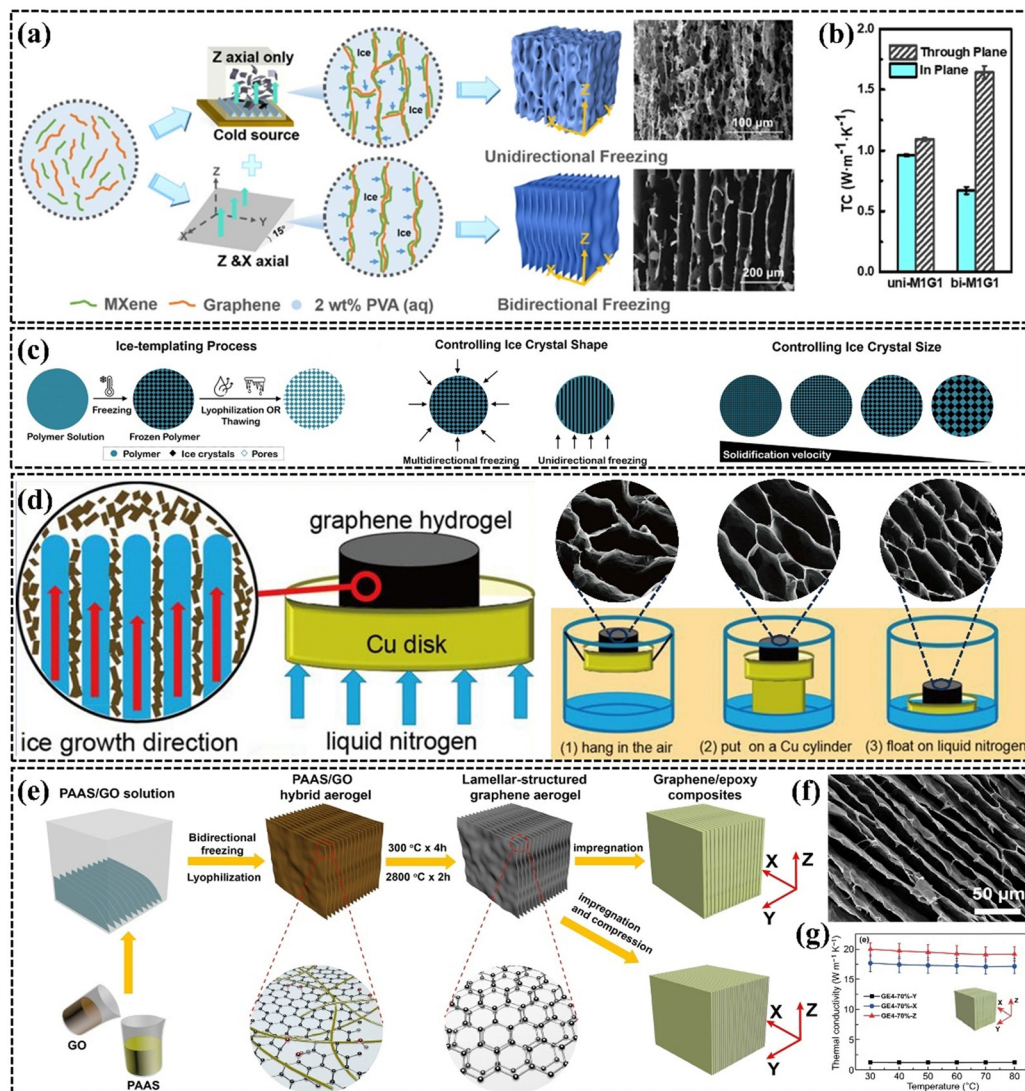


Fig. 10 (a) and (b) Schematic structures and  $k$  values of PEG/MXene/graphene composites obtained by unidirectional and bidirectional freezing (Copyright©2021 American Chemical Society).<sup>152</sup> (c) Effects of cooling rate, solution concentration, and viscosity on pore size and size (Copyright©2021 Wiley-VCH GmbH).<sup>153</sup> (d) Schematic diagram and SEM images of vertically aligned graphene aerogels with different pore sizes fabricated by different directional freezing rates (Copyright©2018 Elsevier Ltd. All rights reserved).<sup>154</sup> (e–g) Schematic illustration of the fabrication, SEM images, and  $k$  of EP/graphene composite (Copyright©2020, The Author(s)).<sup>79</sup>

results indicated that the nanofillers under bidirectional freezing conditions exhibited superior vertical alignment and higher through-plane  $k$  compared to those subjected to unidirectional freezing. This improvement was attributed to the increased temperature gradient in bidirectional freezing, which minimized the branching of the thermal conductivity network, thereby facilitating heat transfer in the vertical direction (Fig. 10(a) and (b)).<sup>152</sup> Cooling rate, solute concentration, and solution viscosity also impact pore size and shape (Fig. 10(c)).<sup>153</sup> Li *et al.* utilized GO hydrogels to create highly aligned graphene aerogels through freeze-drying and carbonization. By adjusting the freezing rate during the process, they achieved vertically aligned graphene aerogels with varying pore sizes. The resulting porous skeleton with smaller pores, prepared by direct contact with liquid nitrogen, displayed optimal

anisotropic  $k$  ( $6.57 \text{ W m}^{-1} \text{K}^{-1}$ ), over 37 times higher than EP (Fig. 10(d)).<sup>154</sup> The poor contact between the fillers can significantly impede phonon transmission, leading to high interfacial thermal resistance. Consequently, extensive research has been dedicated to improving filler connections through various modification techniques. An *et al.* further improved  $k$  by modifying BN and graphene to create covalently bonded thermally conductive fillers. They prepared a BN/rGO/natural rubber composite with covalent bond links through unidirectional freezing and vacuum impregnation, reducing interfacial thermal resistance and phonon scattering, ultimately achieving enhanced through-surface  $k$ .<sup>155</sup> Numerous studies highlight the importance of densely compacted graphene sheets for efficient heat transfer in aerogels. High filler density and well-contacted graphene sheets reduce phonon scattering and

Table 2 Summary of previously reported  $k$  values of polymer composites with rational design of filler distribution

Method	Filler type	Filler content	$k$ ( $\text{W m}^{-1} \text{K}^{-1}$ )		Ref.
			In-plane $k$	Through-plane $k$	
Template method	rGO	1.46 wt%	—	1.50	111
	rGO/GNP	18.1 wt%	—	3	112
	MXene/graphene	18.7 wt%	—	2.44	157
	GO/GNP	—	—	1.82	118
Self-assembly	Graphene	0.86 wt%	—	1.35	86
	GO	2.5 wt%	—	2.53	124
	rGO@Ni(OH)/BN	—	—	2.01	104
	rGO/Al <sub>2</sub> O <sub>3</sub>	—	—	1.68	158
3D printing	BN/multilayer graphene	10 wt%	—	0.69	98
	GNPS	10.93 vol%	—	4.3	126
Vacuum filtration-assisted assembly	Graphene/aramid nanofiber	20 wt%	—	20.54	132
	Alumina/graphene	42.2 wt%	—	13.3	159
	BNNS/graphene/cellulose nanofiber	—	125.0	2.1	160
Layer-by-layer self-assembly	rGO	2.53 wt%	—	2.03	134
	CNT/graphene	—	—	1056	101
Evaporation-assembled	Graphene/CNT	—	1597	2.65	137
External fields assisted alignment	GNP	0.5 vol%	—	0.19	147
	rGO@Fe <sub>3</sub> O <sub>4</sub>	30 wt%	—	0.611	148
Ice-template	BNNS/graphene	11.2 vol%	2.23	1.09	154
	BN/rGO	2.30 vol%	—	20.0	155
	GO/BNNS	—	—	1.49	99

enhance  $k$ . Liu *et al.* drew inspiration from densely stacked high-quality graphene films to produce graphene aerogels with continuous pearl-like layer structures. These graphene/EP composites, with vertically aligned and tightly stacked high-quality graphene flakes, exhibited exceptional through-plane  $k$  ( $\sim 20 \text{ W m}^{-1} \text{K}^{-1}$ ) and significant thermal conductivity enhancement TCE ( $\sim 9915\%$ ) at low graphene loading (Fig. 10(e)–(g)).<sup>79</sup> The ice template method, which has undergone continuous improvements, has achieved significant breakthroughs in the preparation of GPNs with high  $k$ . However, several challenges remain. The mechanical properties of aerogels after freeze-drying are often suboptimal, which significantly limits the applicability of GPNs. Furthermore, this method typically requires coupling with a freeze-drying process, resulting in less efficient GPN preparation. Additionally, overcoming the limitations of pore size continues to be a challenge. Currently, the method can only produce cryogels with micrometer-sized pores, and effectively reducing the pore size to a submicrometer is difficult due to the aggregation of ice crystals.<sup>156</sup>

In addition to the methods mentioned above, there are numerous techniques available for aligning graphene. These methods can be interchanged or combined under appropriate conditions. Detailed literature examples and summaries of the advantages and disadvantages of these graphene alignment techniques are provided in Table 2 and Fig. 11, respectively. These summaries are helpful for researchers to understand and appropriately utilize the alignment technology of graphene.

## 4. GPNs for thermal management applications

### 4.1 Thermal interface materials

The continuous miniaturization of electronic chips has led to a dramatic increase in concentrated heat generation

power,<sup>31,161,162</sup> which can affect the lifetime and product performance of electronic devices.<sup>163,164</sup> The air with extremely low  $k$  present between the heat sink and the heat source can prevent electronic devices from dissipating heat efficiently, so TIM is commonly used to replace air as the heat transfer bridge between the heat source and the heat sink to effectively improve the problem of low heat dissipation efficiency (Fig. 12(a)).<sup>165</sup> However, the TIMs with low  $k$  have emerged as a key challenge to address to guarantee the performance, longevity, and dependability of electronic devices.<sup>5,21,166,167</sup> Ideal TIMs require both high  $k$  and good mechanical compliance. High  $k$  facilitates rapid heat transfer between the heat source and the heat sink, and good mechanical compliance ensures that the TIM adequately fills the interfacial micro void thereby reducing the contact thermal resistance. Common TIMs are mainly composed of thermally conductive fillers (*e.g.*, Al<sub>2</sub>O<sub>3</sub>, AlN, and metal particles) and polymer (*e.g.* PDMS, EP, and SR),<sup>168</sup> and there is a trade-off between  $k$  and mechanical compliance in such filling systems.<sup>169,170</sup> Graphene is a commonly used thermally conductive filler in TIMs due to its ultra-high  $k$  and its ease of modulation into different structures from micro to macro. GPNs filled with different situations have been commonly used for thermal interface thermal conductivity applications in recent years, exhibiting high  $k$ , excellent flexibility, good processability, and low density.<sup>48,171–174</sup>

Common TIMs include both uncured and cured GPNs. Uncured TIMs are recognized for their excellent wettability and flowability, effectively filling gaps between rough surfaces. The viscosity of uncured TIMs is a critical factor influencing their thermal properties, affecting bond line thickness (BLT) and TIM volume. Lower viscosity may reduce BLT but can also lead to leakage.<sup>178</sup> Lewis *et al.*<sup>166</sup> noted that although commercially available uncured TIMs typically begin with high viscosity, the incorporation of a small amount of graphene significantly enhances thermal conductivity, as demonstrated

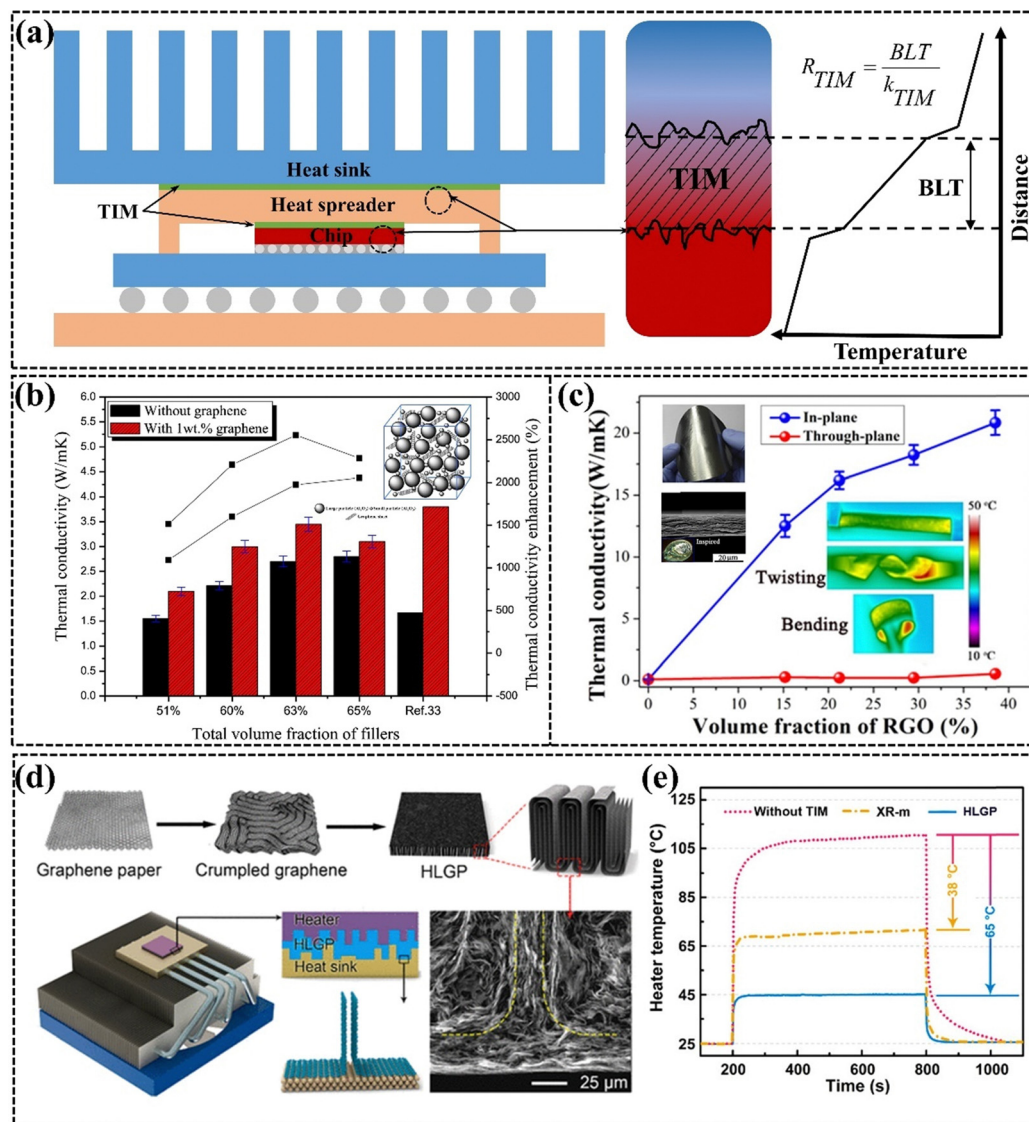
Advantages and Disadvantages of Graphene Alignment Technology				
3D alignment	<b>Salt templated</b> <ul style="list-style-type: none"> <li>✓ Operationally simple;</li> <li>✓ Environmentally friendly;</li> <li>✓ Scalable;</li> <li>✗ The formwork is difficult to remove;</li> <li>✗ Low thermal conductivity;</li> </ul>	<b>Bubble template</b> <ul style="list-style-type: none"> <li>✓ Operationally simple;</li> <li>✓ Environmentally friendly;</li> <li>✓ Scalable;</li> <li>✗ Low thermal conductivity;</li> </ul>	<b>Ni Templated</b> <ul style="list-style-type: none"> <li>✓ High quality;</li> <li>✗ Complex;</li> <li>✗ Expensive;</li> <li>✗ Time-consuming;</li> </ul>	
	<b>Polymer template</b> <ul style="list-style-type: none"> <li>✓ Operationally simple;</li> <li>✓ High quality</li> <li>✗ Noxious;</li> <li>✗ Unevenly dispersed</li> </ul>	<b>Self-assembly</b> <ul style="list-style-type: none"> <li>✓ Operationally simple;</li> <li>✓ Mature technique</li> <li>✗ Poor mechanical strength;</li> <li>✗ Holes are difficult to adjust</li> </ul>	<b>3D printing</b> <ul style="list-style-type: none"> <li>✓ Precisely adjustable</li> <li>✗ Expensive;</li> <li>✗ High selectivity for polymer matrices</li> </ul>	
Horizontal alignment	<b>Vacuum filtration assisted assembly</b> <ul style="list-style-type: none"> <li>✓ Simple and effective;</li> <li>✓ Low costs</li> <li>✗ The filtration rate requirements are high;</li> <li>✗ Scalable</li> </ul>	<b>Layer-by-layer assembly</b> <ul style="list-style-type: none"> <li>✓ Precisely adjustable</li> <li>✗ Scalable;</li> <li>✗ Poor mechanical strength</li> </ul>	<b>Solvent evaporation</b> <ul style="list-style-type: none"> <li>✓ Operationally simple;</li> <li>✓ Scalable</li> <li>✗ Inefficient;</li> <li>✗ Solvent and evaporation conditions need to be strictly controlled</li> </ul>	<b>Hot compression</b> <ul style="list-style-type: none"> <li>✓ Scalable;</li> <li>✓ Excellent mechanical performances</li> <li>✗ The range of available polymers is limited;</li> <li>✗ Expensive</li> </ul>
	<b>Flow-field-induced alignment</b> <ul style="list-style-type: none"> <li>✓ Operationally simple</li> <li>✗ The alignment structure is heterogeneous</li> </ul>	<b>Electric-field-induced alignment</b> <ul style="list-style-type: none"> <li>✓ Remotely controllable;</li> <li>✓ Flexible</li> <li>✗ Susceptible to electrical breakdown;</li> <li>✗ Susceptible to pH and charge</li> </ul>	<b>Magnetic-field-induced alignment</b> <ul style="list-style-type: none"> <li>✓ Flexible;</li> <li>✓ Non-contact;</li> <li>✓ Scalable</li> <li>✗ Higher magnetic field required</li> </ul>	<b>Ice-template</b> <ul style="list-style-type: none"> <li>✓ Flexible;</li> <li>✓ Scalable;</li> <li>✓ Versatility</li> <li>✗ Poor mechanical strength;</li> <li>✗ Time-consuming</li> </ul>
Vertical alignment				

Fig. 11 Detailed literature examples and summary of advantages and disadvantages of graphene alignment technology.

by Yu *et al.*, who showed that adding 1 wt% graphene to silicone grease increased its thermal conductivity from  $2.70 \text{ W m}^{-1} \text{ K}^{-1}$  to  $3.45 \text{ W m}^{-1} \text{ K}^{-1}$  (Fig. 12(b)).<sup>175</sup> Cured TIMs are increasingly preferred in research due to their ease of use and no pump-out effects. They are typically available in two forms, including Graphene pads in block form and graphene paper in film form. Graphene pads are more inclined to transfer heat in the through-plane direction, and graphene needs to be arranged vertically in the matrix to form a vertical heat conduction path. The compressibility of these pads aids in eliminating trapped air between surfaces. Thin graphene paper has garnered attention for its ability to address the low heat transfer efficiency associated with thick adhesive layers in pads. The thickness of graphene paper is typically very minimal. In particular, graphene paper with a bionic nacre layer exhibits exceptionally high in-plane thermal conductivity and tensile strength. Feng *et al.* developed a robust synthetic nacre material by laminating rGO with natural rubber using a straightforward solution casting method. This TIM achieved an impressive heat dissipation rate of  $20.84 \text{ W m}^{-1} \text{ K}^{-1}$  at a

thickness of only  $16\text{--}22 \mu\text{m}$ , while also demonstrating remarkable flexibility and durability, enduring over 10 000 tensile cycles (Fig. 12(c)).<sup>176</sup> Graphene paper can effectively adhere to metal heat sinks, facilitating direct contact between the horizontal graphene and the metal. The superior thermal conductivity of graphene paper, coupled with its ease of large-scale production and low cost, is increasing the potential for practical applications of TIMs in academia and industry. A novel strategy to improve thermal conductivity and reduce contact thermal resistance involves machining horizontal graphene paper into highly conductive graphene pads. Dai *et al.* prepared layered-structured graphene composites through pleating and lateral compression, achieving a vertical alignment of graphene that resulted in a high thermal conductivity of  $143 \text{ W m}^{-1} \text{ K}^{-1}$  and a low compression modulus of  $0.87 \text{ MPa}$ . The cooling efficiency of the graphene pads as a TIM was three times greater than that of leading commercial TIMs, showcasing its superior capability to address interfacial heat transfer challenges in electronic systems (Fig. 12(d) and (e)).<sup>177</sup>





**Fig. 12** (a) Diagram of TIM materials used for chip thermal conductivity and the factors influencing their thermal conductivity. (b) Comparison of the thermal conductivity of silicone thermal grease with and without graphene, and the enhancement achieved with various filler loadings (Copyright © 2015 Elsevier Masson SAS. All rights reserved).<sup>175</sup> (c) The  $k$  of NR/RGO composite films with varying rGO content, with a thickness ranging from 16 to 22 cm (Copyright © 2019 American Chemical Society).<sup>176</sup> (d) Schematic diagram illustrating the structural changes in graphene and the thermal interface material, and (e) the temperature variation of a ceramic heating pad at an applied power of  $20 \text{ W cm}^{-2}$  (Copyright © 2019 American Chemical Society).<sup>177</sup>

## 4.2 Phase change materials

A phase change material is a type of material that undergoes a phase change at a specific temperature or pressure, and the process is usually associated with the absorption or release of a large amount of energy. Polymeric phase change materials are widely used because of their stability and wide range of phase change temperatures.<sup>179</sup> However, the low  $k$  of PCMs is the key issue limiting their development.<sup>179,180</sup> The efficient technique to increase the  $k$  of PCMs is to incorporate highly thermally conductive fillers,<sup>181–183</sup> fins,<sup>184</sup> or thermally conductive porous structures.<sup>185</sup> Graphene nanosheets have been used to enhance the thermal properties of PCMs because of their ultra-high  $k$  and relatively low density. Different forms of graphene-based organic PCMs are often used in the thermal management of

electronic devices,<sup>186,187</sup> battery thermal management,<sup>188,189</sup> and energy storage<sup>190–193</sup> due to their high latent heat and lower contact thermal resistance by improving the wettability of the two contacting interfaces through the solid-to-liquid transition. For example, Li *et al.*<sup>174</sup> incorporated and dispersed a mixture of sulfonated graphene (SG) as a thermally conductive enhancement material in PEG, significantly improving the  $k$  at low SG loading. To enhance the connected thermal pathway, Hussain *et al.*<sup>194</sup> investigated a graphene-coated nickel (GcN) foam composite phase change material demonstrating that attaching graphene to sponge or metal foam is an effective enhancement method. The surface temperature of the battery using GcN foam composite phase change material was reduced by 17% compared to using nickel foam at 1.7 A



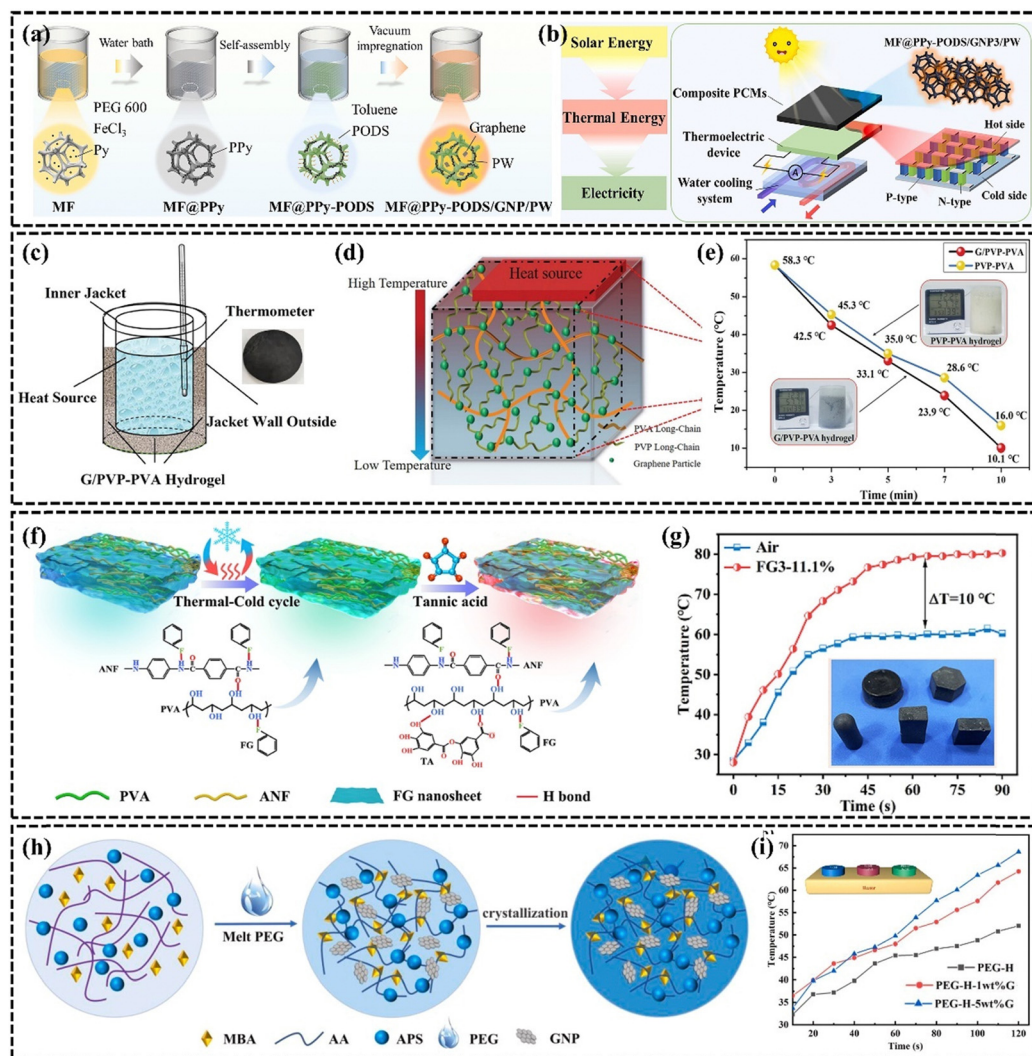


**Fig. 13** (a) Schematic illustration for the preparation process of composite PCMs (Copyright©2022 Elsevier Ltd. All rights reserved).<sup>190</sup> (b) Experimental schematic diagram of the thermoelectric conversion system with composite PCMs driven by solar energy.<sup>190</sup> (c) G/PVP-PVA hydrogel heat dissipation model setup (Copyright©2022 The Authors. Macromolecular Materials and Engineering published by Wiley-VCH GmbH).<sup>195</sup> (d) Mechanism diagram of G/PVP-PVA hydrogel heat dissipation.<sup>195</sup> (e) Comparison of heat dissipation performance of G/PVP-PVA hydrogel and PVP-PVA hydrogel.<sup>195</sup> (f) Schematic preparation procedure of ANF-FG-PVA composite hydrogels (Copyright©2024, American Chemical Society).<sup>196</sup> (g) Temperature versus time for LED of ANF-FG-PVA hydrogel.<sup>196</sup> (h) Synthesis procedure of the graphene-based phase change material composite hydrogel (Copyright©2021 Elsevier Ltd. All rights reserved).<sup>197</sup> (i) Variation curve of upper surface temperature and heating time of phase change hydrogel composite sample.<sup>197</sup>

discharge current. Graphene helps to enhance the thermal storage rate of phase change materials. Cui *et al.* enhanced the thermal conductivity of graphene-based composite PCMs to  $0.59\text{ W m}^{-1}\text{ K}^{-1}$  and increased solar thermal storage efficiency to 79.36%. This PCM can also be utilized in a solar-powered thermoelectric conversion system, showcasing its application in clean energy (Fig. 13(a) and (b)).<sup>190</sup>

Currently, liquid-gas PCMs with an order of magnitude higher latent heat value show a unique appeal than organic solid-liquid PCMs. Water, as a common liquid-gas phase change material with high latent heat ( $2500\text{ J g}^{-1}$ ), has tremendous advantages in heat transfer and heat dissipation. However, the susceptibility of water to leakage limits its wide application in thermal management. Hydrogel is a polymer

formed by physical and chemical cross-linking. The 3D hydrogel network formed by crosslinking and entanglement of polymer chains can store up to 95% of its volume of water,<sup>198</sup> which behaves as a good water storage matrix. In recent years, the use of hydrogels for phase change cooling has become more and more acceptable to the public. Boon-in<sup>199</sup> prepared a dual network hydrogel of PAMPS and PNIPAM to dissipate heat by water evaporation, thus contributing to the relief of pain caused by inflammation of human skin. To accelerate the evaporation of water to achieve the effect of rapid cooling, the addition of fillers to increase the  $k$  of the hydrogel is the main method.<sup>200</sup> Ma *et al.*<sup>195</sup> constructed a highly thermally conductive graphene-based/polyvinylpyrrolidone-poly(vinyl alcohol) (G/PVP-PVA) hydrogel with an interpenetrating network by

physical cross-linking and freeze-thawing combined methods (Fig. 13(c)–(e)). Due to the homogeneous dispersion of graphene in the hydrogel and the formation of thermally conductive pathways, the  $k$  of this hydrogel was as high as  $1.486 \text{ W m}^{-1} \text{ K}^{-1}$ , which was enhanced by 170.18% compared with the  $k$  of the conventional hydrogel ( $0.55 \text{ W m}^{-1} \text{ K}^{-1}$ ). Due to the high latent heat and high  $k$ , the cooling rate of graphene-based hydrogels is as high as  $1.1 \text{ }^{\circ}\text{C min}^{-1}$  far higher than that of commercial gels at  $0.27 \text{ }^{\circ}\text{C min}^{-1}$ . The enhanced  $k$  of hydrogels proves to be crucial for realizing highly efficient heat transfer performance. To broaden the application of hydrogels for the thermal management of flexible electronics, Tian *et al.*<sup>196</sup> created a solid-liquid interpenetrating network hydrogel (ANF-FG-PVA) with a high  $k$  of  $1.42 \text{ W m}^{-1} \text{ K}^{-1}$ , composed of aromatic polyamide nanofibers, fluorinated graphene, and PVA (Fig. 13(f) and (g)). The hydrogel significantly reduced the

operating temperature in the thermal performance test of LEDs. The composite of PCM and hydrogel is also a new PCM. Yang *et al.*<sup>197</sup> incorporated solid-liquid phase change materials into a graphene-based hydrogel and designed a phase change composite with low contact thermal resistance and high  $k$ . The crosslinked network of the hydrogel solves the leakage problem of the phase change material, and the addition of graphene helps to enhance the  $k$  and thermal stability of the composite (Fig. 13(h) and (i)). These approaches are anticipated to significantly advance the development of PCM in the field of thermal management.

### 4.3 Intelligent responsive thermal management materials

A great deal of research has been done on flexible GPNs with high  $k$ , which have displayed good potential for thermal management material applications in many fields. However, with

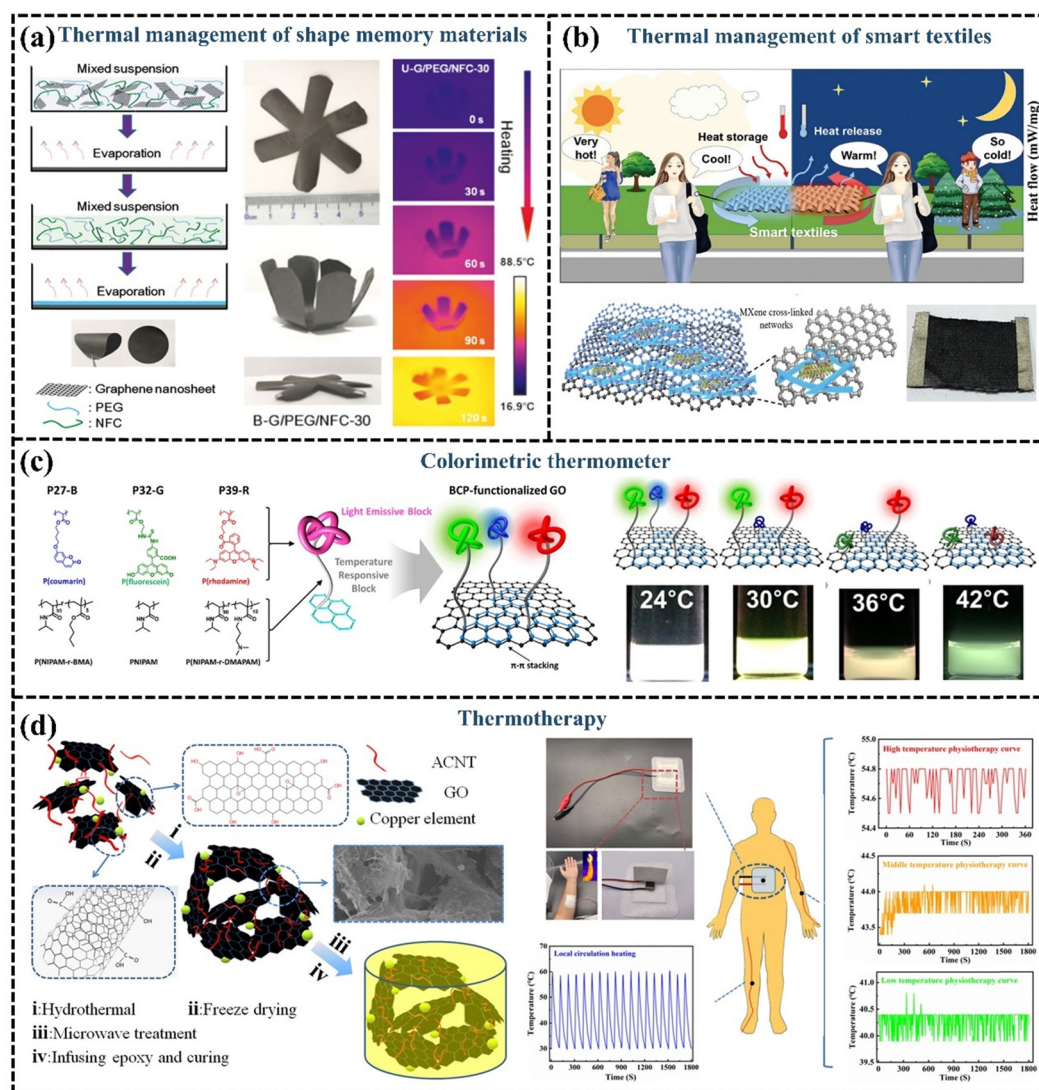


**Fig. 14** (a) Schematic illustration of the evaporation-induced self-assembly process and shape memory behaviors of the hybrid films (Copyright©2019 American Chemical Society).<sup>201</sup> (b) Schematic illustration of the heat storage and temperature regulation of PCM-integrated smart textile (Copyright©2023 Wiley-VCH GmbH).<sup>203</sup> (c) Schematic illustration of the colorimetric thermometer (Copyright©2016, American Chemical Society).<sup>204</sup> (d) Diagrammatic preparation processing and hyperthermia application of the GO-CNT/EP nanocomposites (Copyright©2021 Wiley-VCH GmbH).<sup>205</sup>

the development of microelectronics and other technologies, the smartness of the materials has also become a popular pursuit. It has been proposed that GPN films can be endowed with intelligence by employing shape memory polymers. For example, polyvinyl alcohol is commonly used as a thermally responsive shape memory material, with nanofibrillated cellulose supporting and encapsulating the PEG, and a regular arrangement of graphene to enhance  $k$ . The incorporation of 30 wt% graphene significantly improves the thermal conductivity of GPN films, increasing it to  $21.83 \text{ W m}^{-1} \text{ K}^{-1}$ . The shape memory polymer with high  $k$  is applied to the back of the LED as a lateral heat spreader, effectively reducing the temperature of the LED system and slowing its heating rate, thereby protecting and extending the lifespan of the electronics. Furthermore, the shape memory film begins to expand at  $60^\circ\text{C}$ , providing a visual warning that the LED is overheating. This shape memory polymer exhibits different folding degrees with temperature changes and accelerates the reduction of LED operating temperature, demonstrating excellent capability for smart thermal management (Fig. 14(a)).<sup>201,202</sup>

GPNs are not only used for thermal management in smart electronic devices but are also widely applied in smart textiles. Circuits in wearable electronic devices or electronic smart textiles generate heat during operation, which requires the enhancement of material thermal conductivity for thermal management. The incorporation of graphene with high  $k$  into conventional textiles can be used for heat dissipation and adaptive cooling.<sup>206</sup> Yang *et al.* developed a graphene paper with high out-of-plane  $k$ , flexibility, and a large ultra-thin surface area. They demonstrated that this graphene paper can be utilized as a wearable fabric, exhibiting excellent cooling capabilities under moderate temperature conditions ( $15\text{--}30^\circ\text{C}$ ). Due to its high  $k$ , graphene paper facilitates passive cooling by transferring heat from the body to the environment. This innovative material significantly reduces the cooling response time for individuals, decreasing it from 150 seconds to just 7 seconds when compared to conventional cotton fabrics, highlighting its substantial potential for human body cooling.<sup>207</sup> In addition to its applications in body cooling, smart textiles made from GPNs also show considerable promise in temperature regulation. Chen *et al.* assembled 1D AgNWs, 2D MXene, and graphene on PU fibers LBL alternately to prepare and obtain a smart textile, which exhibited a fast response to both electrical and optical stimuli due to fast electron/phonon transport conferred by graphene. Smart responsive textiles integrated with PCMs can release stored solar energy during the night or on rainy days, enabling continuous self-powered thermoregulation (Fig. 14(b)).<sup>203</sup>

Smart responsive GPNs are also being continuously pioneered for applications in other special scenarios for thermal management. Lee *et al.*<sup>204</sup> developed a colorimetric thermometer based on block copolymer-functionalized graphene, where different block copolymers provide different color display responses as the temperature changes, demonstrating the potential of this material for fluorescent thermo-responsive switching or sensor applications (Fig. 14(c)). In recent years

thermotherapy has become one of the common means used to induce the death of cancer cells and enhance the effect of radiotherapy. Wang *et al.*<sup>205</sup> designed a poly(vinyl alcohol) aerogel consisting of a combination of GO, acidified CNTs, and copper particles as a reinforcement material, which had efficient electrical heating properties, rapid thermal responsiveness, and temperature stability, and the temperature was always maintained in high-temperature thermotherapy at  $54.4\text{--}54.8^\circ\text{C}$ . Thus, thermo-responsive GPNs can fulfill the requirements of thermotherapy devices and have the potential for use in the field of thermotherapy (Fig. 14(d)).

## 5. Conclusions and perspectives

The recent progress in the study of the thermal conductivity of GPNs in recent years is presented from three primary perspectives. This aims to offer insights for the development of the next generation of highly thermally conductive polymer composites that can effectively meet the demand for efficient heat dissipation. In the first part, the primary focus is on a microscopic perspective to analyze the effect of graphene nanosheets on the  $k$  of GPNs. The effects of structural parameters of graphene (*e.g.*, defects, size, and number of layers) on the intrinsic  $k$  of graphene are presented. Common strategies used in recent years to modulate the structural parameters, defects, and surface states of graphene are summarized. These strategies include the exfoliation and preparation of graphene, defect engineering, and surface modification. The distribution state of graphene in the polymer matrix and the effect on thermal conductivity are also fully discussed. In the second part, the discussion primarily adopts a macro perspective. We summarize the preparation of macroscopic thermally conductive structures in GPNs, including hybridization of thermally conductive fillers, 3D network alignment, horizontal alignment, and vertical alignment. The hybridization includes the strategy of hybridizing graphene nanosheets with 0D, 1D, and 2D thermally conductive fillers, respectively, all of which exhibit synergistic effects in the polymer composites. This is because multiple fillers with different shapes can enhance each other's dispersion and enable the construction of thermally conductive pathways by bridging and filling the voids. 3D network alignment, horizontal alignment, and vertical alignment allow the construction of continuous thermally conductive pathways in polymers, overcoming the large thermal resistance caused by discontinuous fillers. In the third part, we summarize some recent applications of GPNs as TIMs, PCMs, and smart responsive thermal management materials in the field of thermal management. Although significant progress has been made in recent years to enhance the  $k$  of GPNs through both micro- and macro-level strategies, there remains considerable opportunity for future research and development.

(1) Graphene is challenging to disperse effectively. To enhance its dispersibility, functionalization is often employed. However, this approach can introduce defects that increase phonon scattering within the graphene structure. A common



alternative is the reduced GO, which aims to improve dispersibility while minimizing defects. Unfortunately, this method typically only partially restores the thermal conductivity of graphene. Additionally, new defects may arise during the reduction process, or the original graphene layer may become inhomogeneous, adversely affecting the material's overall performance. Consequently, the pursuit of improved graphene dispersion while maintaining its intrinsic thermal conductivity is a critical focus in the advancement of GPNs.

(2) In numerous studies, it is evident that authors lack stringent criteria for defining graphene. For instance, graphene can be categorized based on the number of layers into single-layer graphene, double-layer graphene, and multi-layer graphene, *etc.* However, the current definitions of these categories remain rather ambiguous. Additionally, graphene can be classified according to its functionalization into graphene, GO, and rGO. Nevertheless, many researchers may collectively refer to all of these as graphene in their descriptions. Each type of graphene possesses distinct properties that may be suitable for various applications. The absence of standardized information can mislead or confuse readers, thereby impeding the advancement of research. Consequently, the accurate selection of the appropriate type of graphene is essential for success, and the standardization of graphene definitions is particularly urgent.

(3) Model the thermal conductivity pathways of graphene. Parameters such as the length and thickness of the pathway are calculated by constructing a topological model to find the optimal solution or trend. Theoretical guidance can be given to practical experiments through calculations and simulations, which can greatly improve the research efficiency.

(4) In practical applications, thermal conductivity is not the unique indicator for assessing the quality of GPNs. At present, many researchers are overly focused on achieving high  $k$ , often neglecting the importance of other essential properties. In thermal management applications, factors such as thermal stability, heat resistance, mechanical properties, coefficient of thermal expansion, and interfacial characteristics also play a crucial role. For instance, commonly used TIM materials often require both high thermal conductivity and excellent mechanical compliance to ensure efficient heat transport under high packaging pressures. Therefore, when evaluating a material's performance, it is vital to consider multiple parameters and real-world application scenarios to obtain a comprehensive understanding of its behavior under specific conditions. This multidimensional evaluation approach will facilitate more accurate selection and design of materials to meet specific requirements.

(5) The multifunctional integration of GPNs is crucial for enhancing their performance and expanding their range of applications. By incorporating various functions and properties into a single material, it becomes possible to satisfy the increasingly stringent demands for material performance in contemporary society. For instance, imparting self-healing and adhesion properties to GPNs can significantly improve their heat transfer stability during use, thereby greatly reducing the risks associated with accidental damage. Thus, multifunctional

integrated GPNs will further broaden the range of applications for GPNs.

## Data availability

No primary research results, software or code have been included and no new data were generated or analysed as part of this review.

## Conflicts of interest

There are no conflicts to declare.

## Acknowledgements

We acknowledge financial support from the National Natural Science Foundation of China (grant no. 52375221 and 52105229).

## References

- 1 Z. Yuan, H. Ma, M. A. Hussien and Y. Feng, *Macromol. Mater. Eng.*, 2021, **306**, 2100428.
- 2 X. Zhang, Z. Ji, J. Wang and X. Lv, *Appl. Therm. Eng.*, 2023, **235**, 121294.
- 3 L. Lv, J. Ying, L. Chen, P. Tao, L. Sun, K. Yang, L. Fu, J. Yu, Q. Yan, W. Dai, N. Jiang and C.-T. Lin, *Nanomaterials*, 2023, **13**, 793.
- 4 J. Janting, J. G. Theander and H. Egesborg, *IEEE Trans. Device Mater. Reliab.*, 2019, **19**, 313–321.
- 5 J. Chen, X. Huang, B. Sun and P. Jiang, *ACS Nano*, 2019, **13**, 337–345.
- 6 F. Tarannum, R. Muthaiah, R. S. Annam, T. Gu and J. Garg, *Nanomaterials*, 2020, **10**, 1291.
- 7 C. Huang, X. Qian and R. Yang, *Mater. Sci. Eng., R*, 2018, **132**, 1–22.
- 8 C. Zhu, T. Liu, F. Qian, T. Y.-J. Han, E. B. Duoss, J. D. Kuntz, C. M. Spadaccini, M. A. Worsley and Y. Li, *Nano Lett.*, 2016, **16**, 3448–3456.
- 9 D. Li, T. Li, Z. Mao, Y. Zhang and B. Wang, *RSC Adv.*, 2023, **13**, 27599–27607.
- 10 A. K. Tareen, K. Khan, M. Iqbal, Y. Zhang, J. Long, F. Nazeer, A. Mahmood, N. Mahmood, Z. Shi, C. Ma, W. Huan, M. F. Khan, J. Yin, C. Li and H. Zhang, *J. Mater. Chem. C*, 2022, **10**, 11472–11531.
- 11 Y. Zhu, Y. Ming, J. Sun, S. Li, S. Li, H. Xiao, B. Wang and Y. Duan, *Chem. Eng. J.*, 2023, **474**, 145583.
- 12 S. Wan, L. Jiang and Q. Cheng, *Matter*, 2020, **3**, 696–707.
- 13 M. Usman, I.-H. Kim and H.-J. Jung, *AIP Adv.*, 2016, **6**, 055027.
- 14 X. Zhang and P. Samori, *ChemNanoMat*, 2017, **3**, 362–372.
- 15 Q. Guo, J. Guo, H. Chen, P. Zhou, C. Li, K. Yang, N. Hua, J. Wang and M. Weng, *J. Mater. Chem. A*, 2023, **11**, 11773–11785.

- 16 X. Huang, C. Zhi, Y. Lin, H. Bao, G. Wu, P. Jiang and Y.-W. Mai, *Mater. Sci. Eng., R*, 2020, **142**, 100577.
- 17 J. Chen and J. Han, *Results Phys.*, 2019, **15**, 102803.
- 18 J. Chen, X. Gao and W. Song, *Results Phys.*, 2019, **15**, 102771.
- 19 S. Wilczewski, K. Skórczewska, J. Tomaszewska, M. Osial, A. Dąbrowska, K. Nikiforow, P. Jencyk and H. Grzywacz, *Molecules*, 2023, **28**, 3383.
- 20 P. Govindaraj, A. Sokolova, N. Salim, S. Juodkazis, F. K. Fuss, B. Fox and N. Hameed, *Composites, Part B*, 2021, **226**, 109353.
- 21 Z. Wang, Z. Wu, L. Weng, S. Ge, D. Jiang, M. Huang, D. M. Mulvihill, Q. Chen, Z. Guo, A. Jazzar, X. He, X. Zhang and B. B. Xu, *Adv. Funct. Mater.*, 2023, **33**, 2301549.
- 22 F. Zhang, Y. Feng and W. Feng, *Mater. Sci. Eng., R*, 2020, **142**, 100580.
- 23 P. Liu, L. Wang, B. Cao, L. Li, K.-L. Zhang, X.-M. Bian and Z.-L. Hou, *J. Mater. Chem. C*, 2017, **5**, 6745–6754.
- 24 Q. Kong, X. Shi, W. Ma, F. Zhang, T. Yu, F. Zhao, D. Zhao and C. Wei, *J. Hazard. Mater.*, 2021, **415**, 125690.
- 25 H. Chen, V. V. Ginzburg, J. Yang, Y. Yang, W. Liu, Y. Huang, L. Du and B. Chen, *Prog. Polym. Sci.*, 2016, **59**, 41–85.
- 26 R. Wang, C. Xie, B. Gou, H. Xu, S. Luo, J. Zhou and L. Zeng, *Polym. Test.*, 2020, **89**, 106574.
- 27 N. Burger, A. Laachachi, M. Ferriol, M. Lutz, V. Toniazio and D. Ruch, *Prog. Polym. Sci.*, 2016, **61**, 1–28.
- 28 H. Kim, G. Park, S. Park and W. Kim, *ACS Nano*, 2021, **15**, 2182–2196.
- 29 Y. Zhang, Q. Wan and N. Yang, *Small*, 2019, **15**, 1903780.
- 30 J. Chen and B. Liu, *Phys. E*, 2022, **139**, 115146.
- 31 J. Ying, W. Dai, J. Yu, N. Jiang, C.-T. Lin and Q. Yan, *Sci. China: Phys., Mech. Astron.*, 2022, **65**, 117005.
- 32 Z. Ma, Z. Guo, H. Zhang and T. Chang, *AIP Adv.*, 2017, **7**, 065104.
- 33 R. Muthaiah, F. Tarannum, S. Danayat, R. S. Annam, A. S. Nayal, N. Yedukondalu and J. Garg, *Phys. Chem. Chem. Phys.*, 2022, **24**, 14640–14650.
- 34 H.-Y. Cao, Z.-X. Guo, H. Xiang and X.-G. Gong, *Phys. Lett. A*, 2012, **376**, 525–528.
- 35 R. Su and X. Zhang, *Appl. Therm. Eng.*, 2018, **144**, 488–494.
- 36 M. Li, H. Zhou, Y. Zhang, Y. Liao and H. Zhou, *Carbon*, 2018, **130**, 295–303.
- 37 B. S. Lee, *J. Phys.: Condens. Matter*, 2018, **30**, 295302.
- 38 H. Wang, K. Kurata, T. Fukunaga, X. Zhang and H. Takamatsu, *Int. J. Heat Mass Transfer*, 2017, **105**, 76–80.
- 39 M. D. Bhatt, H. Kim and G. Kim, *RSC Adv.*, 2022, **12**, 21520–21547.
- 40 F. Banhart, J. Kotakoski and A. V. Krasheninnikov, *ACS Nano*, 2011, **5**, 26–41.
- 41 A. Fox, U. Ray and T. Li, *J. Appl. Phys.*, 2018, **125**, 015101.
- 42 X.-F. Peng, X. Zhou, S.-H. Tan, X.-J. Wang, L.-Q. Chen and K.-Q. Chen, *Carbon*, 2017, **113**, 334–339.
- 43 B. Mortazavi and S. Ahzi, *Carbon*, 2013, **63**, 460–470.
- 44 N. Khosravian, M. K. Samani, G. C. Loh, G. C. K. Chen, D. Baillargeat and B. K. Tay, *Comput. Mater. Sci.*, 2013, **79**, 132–135.
- 45 J. Wang, C. Li, Y. Sheng, Y. Su and L. Yang, *Appl. Phys. Lett.*, 2022, **121**, 042202.
- 46 H. Guo, B. Hu, Q. Wang, J. Liu, M. Li and B. Li, *Appl. Surf. Sci.*, 2023, **615**, 156404.
- 47 G. Chang, L. Wang, Y. Zhang, X. Li, K. Chen, D. Kan, W. Zhang, S. Zhang, L. Dong, L. Li, X. Bai, H. Zhang and W. Huo, *ACS Appl. Mater. Interfaces*, 2022, **14**, 56156–56168.
- 48 W. Liang, X. Ge, J. Ge, T. Li, T. Zhao, X. Chen, M. Zhang, J. Ji, X. Pang and R. Liu, *Nanomaterials*, 2019, **9**, 938.
- 49 J. Zhang, T. Chen, S. Liu, Z. Chen, Y. Li, S. Zhu and H. Li, *J. Mater. Chem. A*, 2021, **9**, 27529–27540.
- 50 J. Gu and K. Ruan, *Nano-Micro Lett.*, 2021, **13**, 110.
- 51 J. Wang, P. Ren, F. Ren, G. Zhu, A. Sun and C. You, *J. Mater. Sci.*, 2021, **56**, 7951–7965.
- 52 S. Lin and M. J. Buehler, *Nanotechnology*, 2013, **24**, 165702.
- 53 G. Yang, L. Sang, D. R. G. Mitchell, F. Fei Yun, K. Wai See, A. Jumlat Ahmed, S. Sayyar, A. Bake, P. Liu, L. Chen, Z. Yue, D. Cortie and X. Wang, *Chem. Eng. J.*, 2022, **428**, 131205.
- 54 T. Zhou, Y. Du, C. Zhao, Y. Wang and J. Zhao, *Int. J. Energy Res.*, 2020, **44**, 1062–1077.
- 55 C. Zhan, W. Cui, L. Li, X. Quan, Y. Zhang and F. Xiao, *Compos. Sci. Technol.*, 2023, **231**, 109823.
- 56 T. Ma, K. Ruan, Y. Guo, Y. Han and J. Gu, *Sci. China Mater.*, 2023, **66**, 4012–4021.
- 57 A. Chatterjee, R. Verma, H. P. Umashankar, S. Kasthuriengan, N. C. Shivaprakash and U. Behera, *Int. J. Therm. Sci.*, 2019, **136**, 389–395.
- 58 J.-u Jang, S. O. So, J. H. Kim, S. Y. Kim and S. H. Kim, *Compos. Commun.*, 2022, **31**, 101110.
- 59 X. Yang, C. Liang, T. Ma, Y. Guo, J. Kong, J. Gu, M. Chen and J. Zhu, *Adv. Compos. Hybrid Mater.*, 2018, **1**, 207–230.
- 60 J.-u Jang, H. E. Nam, S. O. So, H. Lee, G. S. Kim, S. Y. Kim and S. H. Kim, *Polymers*, 2022, **14**, 323.
- 61 F. Kargar, Z. Barani, R. Salgado, B. Debnath, J. S. Lewis, E. Aytan, R. K. Lake and A. A. Balandin, *ACS Appl. Mater. Interfaces*, 2018, **10**, 37555–37565.
- 62 M. Moniruzzaman and K. I. Winey, *Macromolecules*, 2006, **39**, 5194–5205.
- 63 X. Shen, Z. Wang, Y. Wu, X. Liu, Y.-B. He and J.-K. Kim, *Nano Lett.*, 2016, **16**, 3585–3593.
- 64 A. Wei, Y. Li, W. Ren and W. Ye, *Appl. Phys. Lett.*, 2019, **114**, 021902.
- 65 B. Li and W.-H. Zhong, *J. Mater. Sci.*, 2011, **46**, 5595–5614.
- 66 J. Song and Y. Zhang, *Int. J. Heat Mass Transfer*, 2019, **141**, 1049–1055.
- 67 K. S. Novoselov, A. K. Geim, S. V. Morozov, D. Jiang, Y. Zhang, S. V. Dubonos, I. V. Grigorieva and A. A. Firsov, *Science*, 2004, **306**, 666–669.
- 68 Y.-C. Han, S.-H. Yin, J.-R. Zheng, Y.-F. Hu, L. Sun, L. Zhang, Z.-Q. Tian and J. Yi, *Adv. Funct. Mater.*, 2024, **34**, 2307298.
- 69 X. Li, L. Colombo and R. S. Ruoff, *Adv. Mater.*, 2016, **28**, 6247–6252.
- 70 L. Dong, J. Yang, M. Chhowalla and K. P. Loh, *Chem. Soc. Rev.*, 2017, **46**, 7306–7316.
- 71 C. Xu, R.-S. Yuan and X. Wang, *Carbon*, 2014, **71**, 345.

- 72 L. Zhang, H. Jiao, H. Jiu, J. Chang, S. Zhang and Y. Zhao, *Composites, Part A*, 2016, **90**, 286–295.
- 73 X. Xue, Y. Chen, Q. Yin, X. Zhang, W. Zhang, H. Jia, L. Xiao and L. Hong, *Polym. Int.*, 2018, **67**, 1401–1409.
- 74 N.-J. Song, C.-M. Chen, C. Lu, Z. Liu, Q.-Q. Kong and R. Cai, *J. Mater. Chem. A*, 2014, **2**, 16563–16568.
- 75 B.-Y. Ju, W.-S. Yang, Q. Zhang, M. Hussain, Z.-Y. Xiu, J. Qiao and G.-H. Wu, *Int. J. Miner., Metall. Mater.*, 2020, **27**, 1179–1190.
- 76 I. N. Kholmanov, J. Edgeworth, E. Cavaliere, L. Gavioli, C. Magnuson and R. S. Ruoff, *Adv. Mater.*, 2011, **23**, 1675–1678.
- 77 B. Wang and S. T. Pantelides, *Phys. Rev. B: Condens. Matter Mater. Phys.*, 2011, **83**, 245403.
- 78 G. Xin, T. Yao, H. Sun, S. M. Scott, D. Shao, G. Wang and J. Lian, *Science*, 2015, **349**, 1083–1087.
- 79 P. Liu, X. Li, P. Min, X. Chang, C. Shu, Y. Ding and Z.-Z. Yu, *Nano-Micro Lett.*, 2020, **13**, 22.
- 80 K. K. H. De Silva, H.-H. Huang, R. Joshi and M. Yoshimura, *Carbon*, 2020, **166**, 74–90.
- 81 F. An, X. Li, P. Min, P. Liu, Z.-G. Jiang and Z.-Z. Yu, *ACS Appl. Mater. Interfaces*, 2018, **10**, 17383–17392.
- 82 T.-Y. Wang and J.-L. Tsai, *Comput. Mater. Sci.*, 2016, **122**, 272–280.
- 83 W. Yu, L. Sisi, Y. Haiyan and L. Jie, *RSC Adv.*, 2020, **10**, 15328–15345.
- 84 X. Shen, Z. Wang, Y. Wu, X. Liu and J.-K. Kim, *Carbon*, 2016, **108**, 412–422.
- 85 A. Chandrashekar, M. Hegde, S. Krishna, J. Ayippadath Gopi, T. M. Kotresh and T. N. Prabhu, *Eur. Polym. J.*, 2023, **198**, 112379.
- 86 J. Gong, X. Tan, Q. Yuan, Z. Liu, J. Ying, L. Lv, Q. Yan, W. Chu, C. Xue, J. Yu, K. Nishimura, N. Jiang, C.-T. Lin and W. Dai, *Chin. J. Chem.*, 2022, **40**, 329–336.
- 87 M. Qin, Y. Xu, R. Cao, W. Feng and L. Chen, *Adv. Funct. Mater.*, 2018, **28**, 1805053.
- 88 M.-Y. Song, C.-G. Ma, X.-L. Li, H.-T. Chi, P. Zhang and P.-B. Dai, *Polym. Compos.*, 2023, **44**, 6136–6148.
- 89 J. Huang, W. Yang, J. Zhu, L. Fu, D. Li and L. Zhou, *Composites, Part A*, 2019, **123**, 79–85.
- 90 F. Jiang, X. Cui, N. Song, L. Shi and P. Ding, *Compos. Commun.*, 2020, **20**, 100350.
- 91 X. Zhang, J. Song, J. Meng and K. Zhang, *Materials*, 2022, **15**, 8078.
- 92 Z. Barani, A. Mohammadzadeh, A. Geremew, C.-Y. Huang, D. Coleman, L. Mangolini, F. Kargar and A. A. Balandin, *Adv. Funct. Mater.*, 2020, **30**, 1904008.
- 93 C. Shen, H. Wang, T. Zhang and Y. Zeng, *J. Mater. Sci. Technol.*, 2019, **35**, 36–43.
- 94 R. Lv, H. Guo, L. Kang, A. Bashir, L. Ren, H. Niu and S. Bai, *Nanomaterials*, 2023, **13**, 2243.
- 95 H. Wu, W. Zhou, Q. Liu, X. Cai, Z. Qu, P. Li, D. Hu and X. Jia, *J. Appl. Polym. Sci.*, 2022, **139**, 51838.
- 96 K. Xiong, C. Ma, J. Wang, X. Ge, W. Qiao and L. Ling, *Ceram. Int.*, 2023, **49**, 8847–8855.
- 97 S. Lin, H. Yang, Y. Shen and P. Yang, *Eur. Polym. J.*, 2024, **202**, 112632.
- 98 B. Deng, Y. Shi, X. Zhang, W. Ma, H. Liu and C. Gong, *Nanomaterials*, 2022, **12**, 2335.
- 99 F. Guo, X. Shen, J. Zhou, D. Liu, Q. Zheng, J. Yang, B. Jia, A. K. T. Lau and J.-K. Kim, *Adv. Funct. Mater.*, 2020, **30**, 1910826.
- 100 Y.-Z. Xing, M. Li, H. Jia, L.-J. Xie, D. Liu, Z. Wang, Z.-C. Tao, Y.-L. Tong, Q.-Q. Kong and C.-M. Chen, *J. Mater. Chem. C*, 2024, **12**, 1851–1859.
- 101 D. Hu, W. Gong, J. Di, D. Li, R. Li, W. Lu, B. Gu, B. Sun and Q. Li, *Carbon*, 2017, **118**, 659–665.
- 102 G. K. Dimitrakakis, E. Tylianakis and G. E. Froudakis, *Nano Lett.*, 2008, **8**, 3166–3170.
- 103 Z. Xu, L. Bai, Y. Zhang, J. Cao and J. Zheng, *Compos. Sci. Technol.*, 2023, **240**, 110076.
- 104 Y. Feng, G. Han, B. Wang, X. Zhou, J. Ma, Y. Ye, C. Liu and X. Xie, *Chem. Eng. J.*, 2020, **379**, 122402.
- 105 S. Chen, R. Xu, J. Liu, X. Zou, L. Qiu, F. Kang, B. Liu and H.-M. Cheng, *Adv. Mater.*, 2019, **31**, 1804810.
- 106 D. Suh, C. M. Moon, D. Kim and S. Baik, *Adv. Mater.*, 2016, **28**, 7220–7227.
- 107 X. Du, W. Yang, J. Zhu, L. Fu, D. Li and L. Zhou, *Compos. Sci. Technol.*, 2022, **222**, 109370.
- 108 B. Xie, W. Zhao, X. Luo and R. Hu, *Mater. Sci. Eng., R*, 2023, **154**, 100738.
- 109 H. Ma, B. Gao, M. Wang, Z. Yuan, J. Shen, J. Zhao and Y. Feng, *J. Mater. Sci.*, 2021, **56**, 1064–1086.
- 110 S. Li, W. Wu, D. Drummer, Y. Wang, Z. Lu and X. Zhao, *Polym. Compos.*, 2023, **44**, 5369–5380.
- 111 S. Song, J. Wang, C. Liu, J. Wang and Y. Zhang, *Nanoscale*, 2019, **11**, 15234–15244.
- 112 J. Li, X. Zhao, W. Wu, X. Ji, Y. Lu and L. Zhang, *Chem. Eng. J.*, 2021, **415**, 129054.
- 113 Z. Wang, X. Wang, Z. Zhang, L. Liang, Z. Zhao and J. Shi, *Polym. Compos.*, 2023, **44**, 3610–3621.
- 114 K. Ba, M. Zhang, X. Wang, P. Xu, W. Song, C. Wang, W. Yang and Y. Liu, *Diamond Relat. Mater.*, 2023, **131**, 109585.
- 115 J. Jiang, H. Sun, J. ShangGuan, F. Fu, X. Liu and S. Zhao, *ACS Appl. Mater. Interfaces*, 2022, **14**, 43815–43824.
- 116 L. Pedrazzetti, E. Gibertini, F. Bizzoni, V. Russo, A. Lucotti, L. Nobili and L. Magagnin, *Materials*, 2022, **15**, 1572.
- 117 Z. Chen, W. Ren, L. Gao, B. Liu, S. Pei and H.-M. Cheng, *Nat. Mater.*, 2011, **10**, 424–428.
- 118 J. Yang, G.-Q. Qi, R.-Y. Bao, K. Yi, M. Li, L. Peng, Z. Cai, M.-B. Yang, D. Wei and W. Yang, *Energy Storage Mater.*, 2018, **13**, 88–95.
- 119 J. Yang, X. Shen, W. Yang and J. K. Kim, *Prog. Mater. Sci.*, 2023, **133**, 101054.
- 120 Z. Liu, Y. Chen, Y. Li, W. Dai, Q. Yan, F. E. Alam, S. Du, Z. Wang, K. Nishimura, N. Jiang, C.-T. Lin and J. Yu, *Nanoscale*, 2019, **11**, 17600–17606.
- 121 C. Zhu, X. Lu, H. Wu, X. Hu, X. Li, S. Liu and J.-P. Qu, *Compos. Sci. Technol.*, 2022, **226**, 109532.
- 122 W. Dai, Y. Wang, M. Li, L. Chen, Q. Yan, J. Yu, N. Jiang and C.-T. Lin, *Adv. Mater.*, 2024, **36**, 2311335.
- 123 Z. Yuan, X. Xiao, J. Li, Z. Zhao, D. Yu and Q. Li, *Adv. Sci.*, 2018, **5**, 1700626.



- 124 S. Cui, W. Wu, C. Liu, Y. Wang, Q. Chen and X. Liu, *Nanoscale*, 2021, **13**, 18247–18255.
- 125 C. Zhang, R. Huang, P. Wang, Y. Wang, Z. Zhou, H. Zhang, Z. Wu and L. Li, *ACS Appl. Mater. Interfaces*, 2020, **12**, 58170–58178.
- 126 Q. Lv, Z. Peng, Y. Meng, H. Pei, Y. Chen, E. Ivanov and R. Kotsilkova, *Ind. Eng. Chem. Res.*, 2022, **61**, 16733–16746.
- 127 J. Zhou, X. Wu, Y. Chen, C. Yang, R. Yang, J. Tan, Y. Liu, L. Qiu and H.-M. Cheng, *Adv. Funct. Mater.*, 2022, **32**, 2105879.
- 128 S. Wang, H. He, X. Ye, R. Chen, Q. Li and B. Huang, *Compos. Sci. Technol.*, 2022, **227**, 109591.
- 129 Z. Peng, Q. Lv, J. Jing, H. Pei, Y. Chen and E. Ivanov, *Composites, Part B*, 2023, **251**, 110491.
- 130 Y. Wang, Z. Xu, D. Wu and J. Bai, *Materials*, 2020, **13**, 2406.
- 131 F. Zhang, C. Ye, W. Dai, L. Le, Q. Yuan, K. W. A. Chee, Y. Ke, N. Jiang, C.-T. Lin, Z. Zhan, D. Dai and L. He, *Chin. Chem. Lett.*, 2020, **31**, 244–248.
- 132 X. He, K. Zhang, H. Wang, Y. Zhang, G. Xiao, H. Niu and Y. Yao, *Carbon*, 2022, **199**, 367–378.
- 133 J. Zhu, H. Zhang and N. A. Kotov, *ACS Nano*, 2013, **7**, 4818–4829.
- 134 J. Song, C. Chen and Y. Zhang, *Composites, Part A*, 2018, **105**, 1–8.
- 135 N. Song, D. Jiao, S. Cui, X. Hou, P. Ding and L. Shi, *ACS Appl. Mater. Interfaces*, 2017, **9**, 2924–2932.
- 136 H. Zhu, H. Cao, X. Liu, M. Wang, X. Meng, Q. Zhou and L. Xu, *Mater. Des.*, 2019, **175**, 107783.
- 137 R. Zou, F. Liu, N. Hu, H. Ning, Y. Gong, S. Wang, K. Huang, X. Jiang, C. Xu, S. Fu, Y. Li and C. Yan, *ACS Appl. Mater. Interfaces*, 2020, **12**, 57391–57400.
- 138 K. E. Shopsowitz, H. Qi, W. Y. Hamad and M. J. MacLachlan, *Nature*, 2010, **468**, 422–425.
- 139 H. Zeng, J. Wu, Y. Ma, Y. Ye, J. Liu, X. Li, Y. Wang, Y. Liao, X. Luo, X. Xie and Y.-W. Mai, *ACS Appl. Mater. Interfaces*, 2018, **10**, 41690–41698.
- 140 P. Ding, J. Zhang, N. Song, S. Tang, Y. Liu and L. Shi, *Compos. Sci. Technol.*, 2015, **109**, 25–31.
- 141 Y. Lin, J. Chen, S. Dong, G. Wu, P. Jiang and X. Huang, *J. Mater. Sci. Technol.*, 2021, **83**, 219–227.
- 142 Z. Zhang, J. Qu, Y. Feng and W. Feng, *Compos. Commun.*, 2018, **9**, 33–41.
- 143 V. Ghai, S. Pandit, M. Svensso, R. Larsson, A. Matic, R. Ngaley, S. P. Dash, A. Terry, K. Nygård, I. Mijakovic and R. Kádár, *Adv. Funct. Mater.*, 2024, 2406875.
- 144 A. Sierra-Romero and B. Chen, *Nanocomposites*, 2018, **4**, 137–155.
- 145 M. Monti, M. Natali, L. Torre and J. M. Kenny, *Carbon*, 2012, **50**, 2453–2464.
- 146 C.-S. Lim, A. J. Rodriguez, M. E. Guzman, J. D. Schaefer and B. Minaie, *Carbon*, 2011, **49**, 1873–1883.
- 147 K.-R. Park, H.-B. Cho, M. Lim, B. K. Jang, J. Lee, B. Jeon and Y.-H. Choa, *Appl. Surf. Sci.*, 2021, **551**, 149201.
- 148 J. He, H. Wang, Q. Qu, Z. Su, T. Qin and X. Tian, *Composites, Part A*, 2020, **139**, 106062.
- 149 J. Geng, Y. Men, C. Liu, X. Ge and C. Yuan, *RSC Adv.*, 2021, **11**, 16592–16599.
- 150 M. Li, X. Dai, W. Gao and H. Bai, *Acc. Mater. Res.*, 2022, **3**, 1173–1185.
- 151 M. Li, X. Dai, M. Wang and H. Bai, *Small Methods*, 2024, **8**, 2300213.
- 152 L. Jin, P. Wang, W. Cao, N. Song and P. Ding, *ACS Appl. Mater. Interfaces*, 2022, **14**, 1747–1756.
- 153 H. Joukhdar, A. Seifert, T. Jüngst, J. Groll, M. S. Lord and J. Rnjak-Kovacina, *Adv. Mater.*, 2021, **33**, 2100091.
- 154 X.-H. Li, P. Liu, X. Li, F. An, P. Min, K.-N. Liao and Z.-Z. Yu, *Carbon*, 2018, **140**, 624–633.
- 155 D. An, S. Cheng, Z. Zhang, C. Jiang, H. Fang, J. Li, Y. Liu and C.-P. Wong, *Carbon*, 2019, **155**, 258–267.
- 156 D. Chen, B. Yang, C. Yang, J. Wu and Q. Zhao, *Chin. J. Chem.*, 2023, **41**, 3082–3096.
- 157 L. Jin, W. Cao, P. Wang, N. Song and P. Ding, *Nano-Micro Lett.*, 2022, **14**, 133.
- 158 W. Liang, T. Li, X. Zhou, X. Ge, X. Chen, Z. Lin, X. Pang and J. Ge, *Nanomaterials*, 2020, **10**, 544.
- 159 Y. Chen, X. Hou, M. Liao, W. Dai, Z. Wang, C. Yan, H. Li, C.-T. Lin, N. Jiang and J. Yu, *Chem. Eng. J.*, 2020, **381**, 122690.
- 160 P. Gong, L. Li, M. Li, S. Zhang, F. Yang, Y. Wang, X. Kong, H. Chen, C. Jiao, X. Ruan, T. Cai, W. Dai, Z. Pan, Y. Li, L. Xu, C.-T. Lin, N. Jiang and J. Yu, *Compos. Commun.*, 2023, **40**, 101596.
- 161 W. Hua, L. Zhang and X. Zhang, *J. Mol. Liq.*, 2021, **340**, 117183.
- 162 Y. Xu, X. Wang and Q. Hao, *Compos. Commun.*, 2021, **24**, 100617.
- 163 D.-J. Huang, W.-T. Peng, Y.-T. Lee and M.-C. Lu, *Int. Commun. Heat Mass Transfer*, 2022, **136**, 106193.
- 164 H. Waqas, S. A. Khan, U. Farooq, T. Muhammad, A. Alshehri and S. Yasmin, *Sci. Rep.*, 2022, **12**, 8035.
- 165 H. Zhang, X. Zhang, D. Li, J. Zhuang, Y. Liu, H. Liu, D. Wu, J. Feng and J. Sun, *Adv. Compos. Hybrid Mater.*, 2022, **5**, 1756–1768.
- 166 J. S. Lewis, T. Perrier, Z. Barani, F. Kargar and A. A. Balandin, *Nanotechnology*, 2021, **32**, 142003.
- 167 Y. Wang, Y. Gao, B. Tang, X. Wu, J. Chen, L. Shan, K. Sun, Y. Zhao, K. Yang, J. Yu and W. Li, *RSC Adv.*, 2021, **11**, 25422–25430.
- 168 W. Dai, X.-J. Ren, Q. Yan, S. Wang, M. Yang, L. Lv, J. Ying, L. Chen, P. Tao, L. Sun, C. Xue, J. Yu, C. Song, K. Nishimura, N. Jiang and C.-T. Lin, *Nano-Micro Lett.*, 2022, **15**, 9.
- 169 Y. Wu, C. Zhang, W. Tu, G. Du, X. Zeng, R. Sun, Y. Xu and L. Ren, *Compos. Commun.*, 2023, **37**, 101452.
- 170 Q. Zhang, B. A. Calderon, C. R. Ebbing, L. J. Elston, L. W. Byrd and B.-H. Tsao, *Front. Mater.*, 2020, **7**, 572956.
- 171 P. Zhang, J. Zeng, S. Zhai, Y. Xian, D. Yang and Q. Li, *Macromol. Mater. Eng.*, 2017, **302**, 1700068.
- 172 D. An, Z. Li, H. Chen, C. Liang, Z. Sun, J. Li, J. Yao, Y. Liu and C. Wong, *Composites, Part A*, 2022, **156**, 106890.
- 173 J. Chen and X. Gao, *Diamond Relat. Mater.*, 2019, **100**, 107571.
- 174 J. Zhang, H. Wang, T. Zhang, X. Sun, Y. Meng, C. Ma, T. Zhang, N. Lu, C. Liu and Y. Zeng, *Compos. Sci. Technol.*, 2023, **233**, 109915.

- 175 W. Yu, H. Xie, L. Yin, J. Zhao, L. Xia and L. Chen, *Int. J. Therm. Sci.*, 2015, **91**, 76–82.
- 176 C.-P. Feng, L.-B. Chen, G.-L. Tian, S.-S. Wan, L. Bai, R.-Y. Bao, Z.-Y. Liu, M.-B. Yang and W. Yang, *ACS Appl. Mater. Interfaces*, 2019, **11**, 18739–18745.
- 177 W. Dai, T. Ma, Q. Yan, J. Gao, X. Tan, L. Lv, H. Hou, Q. Wei, J. Yu, J. Wu, Y. Yao, S. Du, R. Sun, N. Jiang, Y. Wang, J. Kong, C. Wong, S. Maruyama and C.-T. Lin, *ACS Nano*, 2019, **13**, 11561–11571.
- 178 S. Sudhindra, L. Ramesh and A. A. Balandin, *IEEE Open J. Nanotechnol.*, 2022, **3**, 169–181.
- 179 J. Pereira da Cunha and P. Eames, *Appl. Energy*, 2016, **177**, 227–238.
- 180 M. Ren, Y. Liu and X. Gao, *Energy*, 2020, **197**, 117262.
- 181 C. Liu, T. Xiao, J. Zhao, Q. Liu, W. Sun, C. Guo, H. M. Ali, X. Chen, Z. Rao and Y. Gu, *Renewable Sustainable Energy Rev.*, 2023, **188**, 113814.
- 182 X. Huang, J. Guo, Y. Yang, S. Li, S. Chen, Y. Liu and S. Zhang, *J. Appl. Polym. Sci.*, 2018, **135**, 46641.
- 183 N. Alizadeh, R. M. Broughton and M. L. Auad, *ACS Appl. Polym. Mater.*, 2021, **3**, 1785–1794.
- 184 J. Jiang, Y. Hong, Q. Li and J. Du, *Energy*, 2023, **283**, 129143.
- 185 W. Lee, J. Hong, J. Song, W. Yang and J. Kim, *Compos. Sci. Technol.*, 2023, **240**, 110092.
- 186 M. Emam, S. Ookawara and M. Ahmed, *Renewable Energy*, 2019, **141**, 322–339.
- 187 G. K. S. Khagokpam and S. Halder, *High Perform. Polym.*, 2018, **31**, 767–777.
- 188 P. Huang, R. Feng, Z. Tang, Y. He, D. Peng, E. Li, M. Wei, Z. He and Z. Bai, *Appl. Therm. Eng.*, 2023, **235**, 121389.
- 189 D. Zou, X. Ma, X. Liu, P. Zheng and Y. Hu, *Int. J. Heat Mass Transfer*, 2018, **120**, 33–41.
- 190 W. Cui, X. Li, X. Li, T. Si, L. Lu, T. Ma and Q. Wang, *J. Cleaner Prod.*, 2022, **367**, 133031.
- 191 S. Wu, T. Yan, Z. Kuai and W. Pan, *Energy Storage Mater.*, 2020, **25**, 251–295.
- 192 A. Allahbakhsh and M. Arjmand, *Carbon*, 2019, **148**, 441–480.
- 193 J. Yang, G.-Q. Qi, Y. Liu, R.-Y. Bao, Z.-Y. Liu, W. Yang, B.-H. Xie and M.-B. Yang, *Carbon*, 2016, **100**, 693–702.
- 194 A. Hussain, I. H. Abidi, C. Y. Tso, K. C. Chan, Z. Luo and C. Y. H. Chao, *Int. J. Therm. Sci.*, 2018, **124**, 23–35.
- 195 J. Ma, W. Du, Z. Chen, W. Wang and L. Zhang, *Macromol. Mater. Eng.*, 2023, **308**, 2200332.
- 196 R. Tian, X. Jia, Y. Bai, J. Yang and H. Song, *ACS Appl. Mater. Interfaces*, 2024, **16**, 1451–1460.
- 197 J. Yang, W. Yu, C. Liu, H. Xie and H. Xu, *Compos. Sci. Technol.*, 2022, **219**, 109223.
- 198 P. Win, C.-G. Lin, Y. Long, W. Chen, G. Chen and Y.-F. Song, *Chem. Eng. J.*, 2018, **335**, 409–415.
- 199 S. Boon-in, M. Theerasilp and D. Crespy, *ACS Appl. Polym. Mater.*, 2023, **5**, 2562–2574.
- 200 J. Yang, W. Yu, Y. Zhang, C. Liu and H. Xie, *Int. Commun. Heat Mass Transfer*, 2021, **127**, 105537.
- 201 S. Cui, F. Jiang, N. Song, L. Shi and P. Ding, *ACS Appl. Mater. Interfaces*, 2019, **11**, 30352–30359.
- 202 Y. Song, F. Jiang, N. Song, L. Shi and P. Ding, *Composites, Part A*, 2021, **141**, 106222.
- 203 X. Chen, Y. He, M. Tian, L. Qu, T. Fan and J. Miao, *Small*, 2023, 2308404.
- 204 J. Lee, H. Yang, C. H. Park, H.-H. Cho, H. Yun and B. J. Kim, *Chem. Mater.*, 2016, **28**, 3446–3453.
- 205 H. Wang, L. Wu, L. Xu, L. Zheng, Y. Wu, K. Wu, J. Wang and Q. Chen, *Adv. Eng. Mater.*, 2021, **23**, 2001429.
- 206 Q. Ge, J. Chu, W. Cao, F. Yi, Z. Ran, Z. Jin, B. Mao, Z. Li and K. S. Novoselov, *Adv. Funct. Mater.*, 2022, **32**, 2205934.
- 207 Y. Guo, C. Dun, J. Xu, J. Mu, P. Li, L. Gu, C. Hou, C. A. Hewitt, Q. Zhang, Y. Li, D. L. Carroll and H. Wang, *Small*, 2017, **13**, 1702645.